Aero-thermo-elastic behaviour of variable stiffness composite laminates and sandwich panels with temperature-dependent material properties

Thin–Walled Structures 224 (2026) 114738

Contents lists available at ScienceDirect

Thin-Walled Structures

journal homepage: www.elsevier.com/locate/tws

Full length article

Aero-thermo-elastic behaviour of variable stiffness composite laminates and sandwich panels with temperature-dependent material properties

J.A. Moreira [a,*], F. Moleiro [a], A.L. Araújo [a], A. Pagani [b]

[a] IDMEC, Instituto Superior Técnico, Universidade de Lisboa, Av. Rovisco Pais 1, 1049-001, Lisboa, Portugal
[b] MUL2, Department of Mechanical and Aerospace Engineering, Politecnico di Torino, Corso Duca degli Abruzzi 24, 10129, Torino, Italy

ARTICLE INFO

Keywords:
Aero-thermo-elasticity
Panel flutter
Thermal buckling
Temperature-dependent material properties
Variable stiffness composites
Sandwich panels

ABSTRACT

This work is focused on the evaluation of the impact of temperature-dependent material properties on the linear aero-thermo-elastic flutter and buckling stability of variable stiffness composite laminates and sandwich panels with curvilinear fibres under supersonic airflow and thermal loads. To ensure a proper structural modelling, an assessment of Equivalent Single Layer and Layerwise models is also provided, involving the First- and Third-order Shear Deformation Theories as well as further refined theories based on high-order Lagrange z-expansions with thickness stretching. Numerical applications are centred on graphite-epoxy composite laminates and PVC foam core sandwich panels, with either unidirectional or curvilinear fibres, considering simply supported and clamped boundary conditions. It is concluded that temperature-dependent material properties can substantially decrease both critical buckling temperatures and flutter boundaries, depending on the fibre orientations, thermal expansion coefficients and boundary conditions. In particular, the temperature-dependency of the core material plays a major role on the aero-thermo-elastic stability of sandwich panels. Ultimately, the models accuracy assessment reveals that high-order theories are necessary to attain highly accurate flutter estimations for temperatures close to the critical buckling temperature, especially when considering curvilinear fibres and temperature-dependent material properties.

1. Introduction

Understanding the aero-thermo-elastic behaviour of advanced materials is crucial for the development of cutting-edge and highly efficient high speed air vehicles with supersonic capabilities. Examples of such materials consist of variable stiffness composites (VSC) with curvilinear fibre paths and functionally graded metal–ceramic mixtures, along with their incorporation into sandwich panels [1]. On the one hand, thin-walled aerospace structures designed for supersonic flight are often exposed to intense aerodynamic and thermal loads, which may give rise to undesirable aero-thermo-elastic instability phenomena, such as thermal buckling and supersonic panel flutter [2–4], i.e. static and dynamic instabilities, respectively. On the other hand, the thermal stresses and thermal degradation of the material properties render detrimental effects to the load-bearing capacity and structural integrity, promoting the occurrence of catastrophic panel flutter at lower airspeeds [5] and post-flutter chaotic motions [6]. More precisely, pioneering investigations by Olsson [7] in the late 1970s, regarding the supersonic flutter of isotropic cylindrical shells, indicate that the inclusion of temperature-dependent material properties can lead to a 30% reduction in the flutter boundaries.

To address critical design criteria, variable stiffness composites (VSC) with carefully tailored curvilinear fibre paths emerge as a highly promising structural design technology, including the optimization of buckling loads and natural frequencies [8,9], critical buckling temperatures [10] and aeroelastic flutter margins in supersonic panels [11]. Even though VSC laminates with curvilinear fibres are advantageous for enhancing structural performance, outperforming conventional composite laminates with unidirectional fibres in many instances, the thermo-mechanical response is still influenced by the temperature-dependent behaviour of the material properties, as highlighted by Li and Nie [10]. Regarding the design of lightweight sandwich panels with soft foam core, the material properties of low density polymeric foams, such as the PVC foams, are also highly sensitive to temperature variations [12], thus decreasing the effective thermo-mechanical characteristics, including buckling loads and natural frequencies [13]. However, the proper structural modelling of highly anisotropic multi-layered composite panels, such as VSC laminates and soft core sandwich panels, requires a careful attention to high-order deformations and discrete layer effects, which is commonly attained by resorting to three-dimensional (3D) models or refined bi- and one-dimensional

* Corresponding author.
E-mail address: joao.anjos.moreira@tecnico.ulisboa.pt (J.A. Moreira).

https://doi.org/10.1016/j.tws.2026.114738
Received 19 October 2025; Received in revised form 7 January 2026; Accepted 26 February 2026
Available online 27 February 2026

(2D and 1D) models involving high-order Layerwise (LW) descriptions with quasi-3D predictive capabilities [14,15]. These modelling challenges are particularly critical when considering pronounced through-thickness inhomogeneities of material properties, intricate in-plane stiffness distributions and thermal loads, thus rendering conventional Equivalent Single Layer (ESL) descriptions based on simpler plate theories as insufficient for fully capturing the thermo-elastic response [16,17].

In the context of thermal buckling analysis, Vescovini and Dozio [17] and Bracaglia et al. [18] applied the Carrera Unified Formulation (CUF) to investigate the role of refined structural theories in the modelling of variable stiffness laminated composite plates under uniform heating, assuming temperature-independent material properties. It is also worth mentioning prior works concerning conventional composite laminates and sandwich plates with unidirectional fibres [19,20]. These studies highlight the importance of employing higher-order structural theories, particularly in scenarios where 3D effects are significant, such as in moderately thick and thick plates, as well as in VSC laminates featuring highly steered fibre paths. The effect of temperature-dependent material properties in the thermal buckling analysis of laminated composite plates with unidirectional fibres is taken into account by Shen [21] and Shariyat [22], considering uniform temperature rise, as well as by Singha et al. [23] for both uniform and linearly varying temperature distributions. In terms of the structural models, ESL descriptions based on shear deformation plate theories devoid of thickness stretching are considered in [21,23], whereas LW descriptions involving refined plate theories with thickness stretching are applied in [22]. Assuming temperature-independent material properties and the First-order Shear Deformation Theory (FSDT), Zhao et al. [24] highlighted that optimized curvilinear fibre orientations, combined with curvilinear stiffeners, enable effective stress redistribution in stiffened laminated plates under thermal loads, leading to higher buckling temperatures than those of conventional designs involving unidirectional fibres and unidirectional stiffeners. Similarly using the FSDT, the thermal buckling behaviour of VSC laminates with temperature-dependent material properties is discussed by Li and Nie [10].

The preliminary aero-thermo-elastic analysis and design of multilayered composite panels subjected to supersonic airflow and thermal environments is commonly carried out under the assumption of temperature-independent properties, while considering classical thin plate theories or shear deformation plate theories without thickness stretching for the structural formulation, and the quasi-steady First-order Piston Theory as aerodynamic model [1]. For example, Jiang and Li [25] applied a finite element (FE) model with Kirchhoff's thin plate theory to investigate the aero-thermo-elastic behaviour of trapezoidal laminated composite panels under supersonic airflow and shock wave effects. Song and Li [26] evaluated the aero-thermo-elastic characteristics of supersonic sandwich composite panels with pyramidal and triangular lattice cores, resorting to the Rayleigh–Ritz method and a LW model involving the FSDT for the core and the Classical Laminated Plate Theory (CLPT) for the skins. Also using the FSDT, Yu et al. [27] applied the isogeometric method for supersonic flutter analysis of thermally loaded laminated composite panels with and without cut-out. Moreover, Zhang et al. [28] focused on the non-linear aero-thermo-elastic flutter analysis of supersonic laminated composite panels under non-smooth frictional boundaries and random acoustic loads, using a FE model involving the Third-order Shear Deformation Theory (TSDT) with zig-zag effects. It is highlighted that both thermal and acoustic loads can affect the post-flutter motion, such that the Limit Cycle Oscillation (LCO) regime can degenerate into unstable chaotic motion. The same conclusion in terms of thermal loads is also emphasized by Ouyang and Liu [29] regarding the non-linear aero-thermo-elastic flutter behaviour of supersonic variable stiffness composite panels. In addition, Gao et al. [30] investigated the thermal buckling and non-linear flutter characteristics of supersonic composite panels, showing that the aero-thermo-elastic stability region where the panel operates without experiencing either flutter or buckling can be improved by considering curvilinear fibres. Gong et al. [31] focused on the linear aero-thermo-elastic flutter analysis of VSC plates supported on elastic foundations. Numerical results indicate that properly tailored curvilinear fibres (usually with larger fibre orientation on the centre and smaller steering on the leading and trailing edges) yield substantially improved flutter and dynamic characteristics relative to conventional composite laminates with unidirectional fibres, whereas an increased shear foundation stiffness markedly enhanced the flutter stability. The previous studies [29–31] considered plate models based on the ESL FSDT. Considering thin shell theory, Chen and Nie [32] and Nie et al. [33] discussed the non-linear flutter behaviour of curved VSC panels, concluding that composite laminates with curvilinear fibres can outperform straight fibre counterparts in flutter resistance, with stiffer elastic boundary supports reducing flutter amplitudes and raising critical pressure. In contrast, greater panel curvature decreases the bifurcation pressure and amplifies post-flutter deflections.

Regarding the application of high-order structural models with thickness stretching for aero-thermo-elastic analysis of supersonic VSC panels, an assessment of 1D CUF models is provided by Yan et al. [34], including both ESL and LW descriptions with linear and quadratic z-expansions of the displacements. In terms of refined 2D FE models, Moreira [35,36] provided an assessment of ESL and LW descriptions aimed for aeroelastic flutter analysis of variable stiffness laminated composite panels and viscoelastic sandwich panels under supersonic airflow. LW models with variable-order shear deformation theories are also explored in the context of active aeroelastic flutter control of smart composite panels [37] and smart viscoelastic sandwich panels with variable stiffness composite skins [38], albeit excluding thermal effects. Moreover, Moreira et al. [39] investigated the aero-thermo-elastic stability of variable stiffness sandwich panels, including linear and sinusoidal fibre angle distributions, but excluding temperature-dependent material properties. Assuming linearly varying temperature-dependent material properties, Chai et al. [40] focused on the non-linear aero-thermo-elastic analysis of supersonic lattice core sandwich panels with unidirectional fibre composite skins, highlighting the advantageous effect of the shearing core layer and the Winkler elastic foundation on the occurrence of post-flutter chaotic motions. It is also worth emphasizing studies focused on the aero-thermo-elastic response of isotropic panels with temperature-dependent material properties [5–7].

Despite growing interest in VSC structures for aerospace applications, the linear aero-thermo-elastic stability behaviour of multilayered VSC panels incorporating temperature-dependent material properties remains largely unexplored. The primary novelty of this work lies in the first comprehensive assessment of thermal degradation effects on the aero-thermo-elastic stability of both curvilinear fibre composite laminates and soft core sandwich panels under supersonic airflow. In particular, this study uniquely explores the combined influence of temperature-dependent material properties, including the critical role of core material degradation in sandwich structures, while highlighting the superior stability performance offered by curvilinear fibre paths over conventional unidirectional fibre configurations. A further distinctive contribution is the systematic comparison of ESL and LW models, encompassing variable-order shear deformation theories without thickness stretching and quasi-3D formulations with high-order Lagrange z-expansions that include thickness stretching. This comparison provides new insight into the modelling accuracy required for reliable aero-thermo-elastic predictions in thermally degraded VSC structures, especially near critical buckling conditions. In line with prior works on panel flutter, the aerodynamic loads generated by the external supersonic airflow are modelled resorting to the quasi-steady First-order Piston Theory, while the thermal load is treated as a predetermined external load. Numerical applications focus on graphite-epoxy composite laminates and PVC foam core sandwich panels, considering unidirectional and curvilinear fibres.

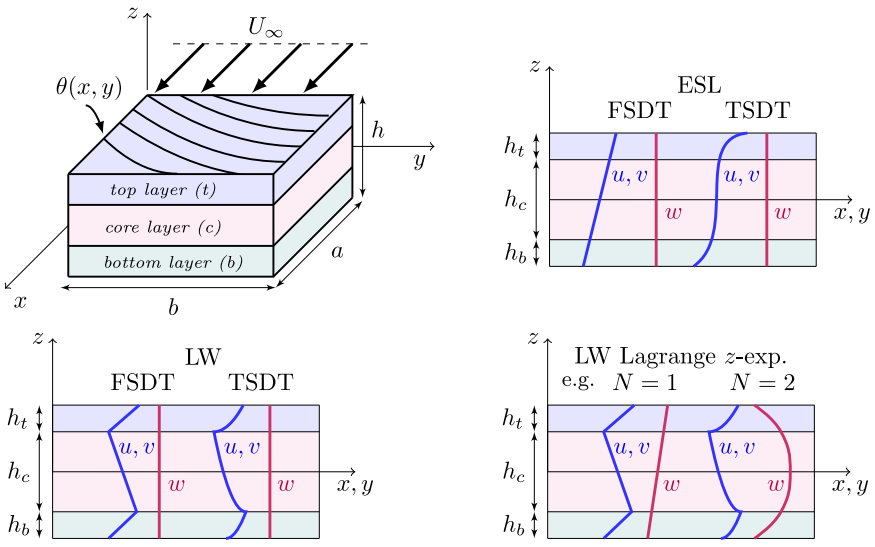

Fig. 1. Illustrative representation of a variable stiffness multilayered composite panel, taken as three discrete layers, under supersonic airflow along the x-axis: geometry and structural theories.

2. Structural modelling

In the present work, the structural modelling of thermally loaded supersonic multilayered panels, namely composite laminates and soft core sandwich panels, is carried out making use of variable-kinematic displacement formulations, encompassing both ESL and LW descriptions. As represented in Fig. 1, the flat panel has in-plane dimensions $a \times b$ and total thickness h, whereas the supersonic airflow is aligned with the x-axis and applied on the upper surface.

More precisely, the LW models are developed under the assumption that the multilayered panel is taken as a set of three perfectly bonded discrete layers, denoted as *top* (t), *core* (c) and *bottom* (b) layers. As illustrated in Fig. 1, the through-thickness distribution of the displacements u, v and w in the x-, y- and z-axis, respectively, are described resorting to either shear deformation plate theories devoid of thickness stretching (FSDT and TSDT) or further refined quasi-3D theories based on variable-order Lagrange z-expansions with thickness stretching. Additionally, it is assumed that the temperature is uniformly distributed, which means that each layer is exposed to the same temperature difference $\Delta\mathcal{T} = \mathcal{T} - \mathcal{T}_0$, where $\mathcal{T}_0$ stands for the stress-free initial reference temperature.

In general, each k-discrete layer illustrated in Fig. 1 can represent a sublaminate with a total of N_p^k physical layers made of composite with curvilinear fibres, thus exhibiting spatially varying orientations $\theta(x,y)$. In line with leading works on composites laminates with curvilinear fibres by Gürdal and Olmedo [41], as also followed in more recent researches [18,35,42], it is considered the case of linear fibre angle distributions along the x-axis, parametrized as follows:

$$\theta(x) = T_0 + \frac{2(T_1 - T_0)}{a}\left|x - \frac{a}{2}\right|, \quad 0 \le x \le a \tag{1}$$

where $T_0 = \theta(a/2)$ and $T_1 = \theta(0) = \theta(a)$ are the fibre orientations at the centre and edges of the panel, respectively. These composite layers are denoted by $\langle T_0, T_1 \rangle$, as illustrated in Fig. 2 for the case of $T_0 = 0°$ and $T_1 = 45°$.

2.1. Shear deformation theories without thickness stretching

The FSDT and TSDT without thickness stretching describe the through-thickness distributions of the in-plane displacements using linear and cubic Taylor z-expansions, respectively, while assuming a constant distribution of the transverse displacement [43]. Even though

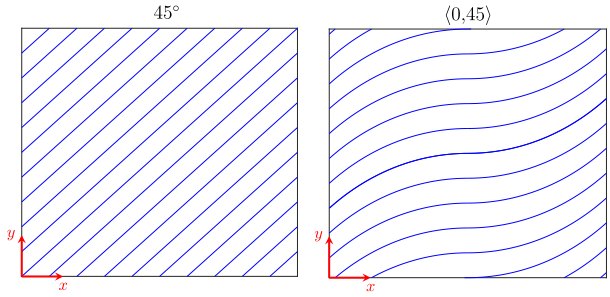

Fig. 2. Composite layers with unidirectional fibres at 45° and curvilinear fibres $\langle 0, 45 \rangle$.

the well-known Koiter recommendations [44] suggest that an improvement of the transverse shear terms should also be accompanied by a refinement of the transverse normal strains, the shear deformation theories devoid of thickness stretching require fewer independent variables than quasi-3D plate theories with thickness stretching, which include more terms in the z-expansion of the transverse displacement.

For the TSDT, the components of the k-discrete layer displacement vector $\boldsymbol{u}^k = \{u^k \; v^k \; w^k\}^T$ are given by:

$$u^k(x,y,z) = u_0^k(x,y) + \left(z - \bar{z}^k\right)\phi_x^k(x,y) + \left(z - \bar{z}^k\right)^2 \varpi_x^k(x,y) + \left(z - \bar{z}^k\right)^3 \psi_x^k(x,y) \tag{2a}$$

$$v^k(x,y,z) = v_0^k(x,y) + \left(z - \bar{z}^k\right)\phi_y^k(x,y) + \left(z - \bar{z}^k\right)^2 \varpi_y^k(x,y) + \left(z - \bar{z}^k\right)^3 \psi_y^k(x,y) \tag{2b}$$

$$w^k(x,y,z) = w_0^k(x,y) \tag{2c}$$

where u_0^k, v_0^k and w_0^k represent the displacements of the k-layer mid-plane (located at $z = \bar{z}^k$), ϕ_x^k and ϕ_y^k stand for the rotations of the normals to the mid-plane about the y- and x-axes, respectively, while ϖ_x^k, ϖ_y^k, ψ_x^k and ψ_y^k denote the higher-order expansion variables. It is important to note that the displacements of the FSDT can be recovered from Eq. (2) by neglecting the high-order terms.

In ESL descriptions, the multilayered panel is modelled by a sole discrete layer, using the displacement variables associated to the middle layer ($k = c$) to describe the whole multilayered panel represented in Fig. 1. Therefore, the discrete layer index k can be omitted, such that the nine degrees of freedom (DOF) associated to the ESL TSDT model

are $\boldsymbol{d} = \{u_0\ v_0\ w_0\ \phi_x\ \phi_y\ \varpi_x\ \varpi_y\ \psi_x\ \psi_y\}^T$, whereas for the ESL FSDT model, only the first five DOF are necessary.

On the other hand, the proposed LW descriptions make use of three discrete layers (Fig. 1), imposing *a priori* the C_z^0 interlaminar continuity conditions of the displacements between adjacent layers. The detailed expressions of the displacements through-thickness distributions utilized in the LW FSDT and LW TSDT models are explicitly outlined in previous works [36,37], being omitted here for brevity. Nonetheless, to be clear, the twenty one DOF involved in the LW TSDT model of the three discrete layers are $\boldsymbol{d} = \{u_0^c\ v_0^c\ w_0^c\ \phi_x^c\ \phi_y^c\ \varpi_x^c\ \varpi_y^c\ \psi_x^c\ \psi_y^c\ \phi_x^t\ \phi_y^t\ \varpi_x^t\ \varpi_y^t\ \psi_x^t\ \psi_y^t\ \phi_x^b\ \phi_y^b\ \varpi_x^b\ \varpi_y^b\ \psi_x^b\ \psi_y^b\}^T$, whereas for the LW FSDT model, no high-order generalized displacement is included and therefore only nine DOF remain, i.e. $\boldsymbol{d} = \{u_0^c\ v_0^c\ w_0^c\ \phi_x^c\ \phi_y^c\ \phi_x^t\ \phi_y^t\ \phi_x^b\ \phi_y^b\}^T$.

In the context of shear deformation plate theories without transverse normal strains ϵ_{zz}, the transverse normal stresses σ_{zz} are also disregarded to avoid thickness locking [14,43]. As a result, the reduced plane stress constitutive equations of the p-physical layer within the k-discrete layer are written in the global reference system (x, y, z) as shown:

$$\begin{Bmatrix} \sigma_{xx}^{kp} \\ \sigma_{yy}^{kp} \\ \sigma_{yz}^{kp} \\ \sigma_{xz}^{kp} \\ \sigma_{xy}^{kp} \end{Bmatrix} = \begin{bmatrix} \bar{Q}_{11}^{kp} & \bar{Q}_{12}^{kp} & 0 & 0 & \bar{Q}_{16}^{kp} \\ \bar{Q}_{12}^{kp} & \bar{Q}_{22}^{kp} & 0 & 0 & \bar{Q}_{26}^{kp} \\ 0 & 0 & \bar{Q}_{44}^{kp} & \bar{Q}_{45}^{kp} & 0 \\ 0 & 0 & \bar{Q}_{45}^{kp} & \bar{Q}_{55}^{kp} & 0 \\ \bar{Q}_{16}^{kp} & \bar{Q}_{26}^{kp} & 0 & 0 & \bar{Q}_{66}^{kp} \end{bmatrix} \begin{Bmatrix} \epsilon_{xx}^{kp} \\ \epsilon_{yy}^{kp} \\ \gamma_{yz}^{kp} \\ \gamma_{xz}^{kp} \\ \gamma_{xy}^{kp} \end{Bmatrix} \tag{3}$$

In short, the previous stress–strain relations are defined using compact notation as follows:

$$\boldsymbol{\sigma}^{kp} = \bar{\boldsymbol{Q}}^{kp} \boldsymbol{\epsilon}^{kp} \tag{4}$$

where $\boldsymbol{\sigma}^{kp}$ and $\boldsymbol{\epsilon}^{kp}$ are the stress and strain components, respectively, structured as vectors, whereas $\bar{\boldsymbol{Q}}^{kp}$ stands for the tensor of reduced elastic coefficients in the global reference system.

Under the assumption of infinitesimal strains, the geometrical strain–displacement relations are the following:

$$\epsilon_{xx} = u_{,x},\ \epsilon_{yy} = v_{,y},\ \epsilon_{zz} = w_{,z} \tag{5a}$$

$$\gamma_{yz} = v_{,z} + w_{,y},\ \gamma_{xz} = u_{,z} + w_{,x},\ \gamma_{xy} = u_{,y} + v_{,x} \tag{5b}$$

When dealing with composite layers featuring spatially varying fibre orientations $\theta(x, y)$, the reduced elastic coefficients in the global reference system are dependent on the in-plane coordinates, i.e. $\bar{\boldsymbol{Q}}^{kp} = \bar{\boldsymbol{Q}}^{kp}(x, y)$, due to the necessary in-plane rotation between the layer material reference system and the global reference system [43]. In addition, by considering temperature-dependent material properties, the reduced elastic coefficients are also dependent on the temperature $\mathcal{T}$, which means that, in the most general case, $\bar{\boldsymbol{Q}}^{kp} = \bar{\boldsymbol{Q}}^{kp}(x, y, \mathcal{T})$. Regarding the LW FSDT model, no shear correction factor is introduced for the evaluation of transverse shear stresses, as also followed by Moreira et al. [35,36], whereas the usual shear correction factor $K_s = 5/6$ is applied in the ESL FSDT model [35,43].

In line with prior works on thermo-mechanical buckling [17–19] and aero-thermo-elastic flutter [26,29,34,39,45], the thermal problem is solved in a decouple framework, treating the effect of the thermal environment as a predetermined external load. In other words, the thermal variables of the problem are known *a priori* and the variational formulation is purely based on displacement variables. Moreover, the thermal buckling analysis is carried out assuming a one-step linearized buckling approach [46], which reduces the stability problem to a linear eigenvalue analysis involving proportional geometric stiffness, such that the critical stress state is linearly dependent on the initial stresses. Under the assumption of uniform temperature difference and stable pre-buckling behaviour, such that the thermal problem can be linearized, the in-plane thermal pre-stresses are evaluated pointwise, at each integration point, accounting for the spatially varying material properties due to curvilinear fibre paths. These thermal pre-stresses contribute to the geometric stiffness matrix, which is subsequently included in the linear eigenvalue problem of the (one-step) thermal buckling analysis or aero-thermo-elastic flutter analysis. Ultimately, this one-step approach allows a direct formulation of the linear eigenvalue problem, without requiring a separate pre-buckling analysis, while still capturing the key effects of variable stiffness on thermal stress distribution and subsequent aero-thermo-elastic response. It is worth noting that, alternatively, a two-step approach could be adopted, in which the pre-buckling thermal stresses – required for constructing the geometric stiffness matrix – are determined *a priori* by solving the non-linear static equilibrium equations under the applied thermal load [46]. The two-step approach would fully account for any out-of-plane deformations and stress distributions, at the expense of increased computational effort.

Considering the one-step approach, the thermal stresses are estimated using the reduced plane stress constitutive equations as shown:

$$\boldsymbol{\sigma}_{\text{th}}^{kp} = \bar{\boldsymbol{Q}}^{kp} \boldsymbol{\epsilon}_{\text{th}}^{kp} = -\bar{\boldsymbol{Q}}^{kp} \bar{\boldsymbol{\alpha}}^{kp} \Delta\mathcal{T} = -\bar{\boldsymbol{\beta}}^{kp} \Delta\mathcal{T} \tag{6}$$

where $\bar{\boldsymbol{\alpha}}^{kp} = \{\bar{\alpha}_{11}^{kp}\ \bar{\alpha}_{22}^{kp}\ 0\ 0\ \bar{\alpha}_{12}^{kp}\}^T$ and $\bar{\boldsymbol{\beta}}^{kp} = \{\bar{\beta}_{11}^{kp}\ \bar{\beta}_{22}^{kp}\ 0\ 0\ \bar{\beta}_{12}^{kp}\}^T$ are the thermal expansion coefficients and thermal stress coefficients written in the global reference system, respectively. Detailed expressions for the thermal expansion coefficients and necessary in-plane rotation are presented explicitly in [43]. In the most general scenario, the applied thermal stresses at the layer level can be composed by in-plane normal stresses σ_{xx}^{kp} and σ_{yy}^{kp} as well as in-plane shear stresses σ_{xy}^{kp}. It is important to emphasize that in the context of spatially varying fibre orientations $\theta(x, y)$ and temperature-dependent material properties, both the thermal expansion coefficients and the thermal stress coefficients are dependent on the in-plane coordinates and temperature, i.e. $\bar{\boldsymbol{\alpha}}^{kp} = \bar{\boldsymbol{\alpha}}^{kp}(x, y, \mathcal{T})$ and $\bar{\boldsymbol{\beta}}^{kp} = \bar{\boldsymbol{\beta}}^{kp}(x, y, \mathcal{T})$.

The evaluation of the virtual work performed by the in-plane thermal stresses in Eq. (6) is carried out taking into account the non-linear terms of the Green–Lagrange in-plane strains, which are given by:

$$\tilde{\epsilon}_{xx} = \frac{1}{2}\left(u_{,x}^2 + v_{,x}^2 + w_{,x}^2\right) \tag{7a}$$

$$\tilde{\epsilon}_{yy} = \frac{1}{2}\left(u_{,y}^2 + v_{,y}^2 + w_{,y}^2\right) \tag{7b}$$

$$\tilde{\gamma}_{xy} = u_{,x}u_{,y} + v_{,x}v_{,y} + w_{,x}w_{,y} \tag{7c}$$

such that the generalized non-linear strain vector is conveniently structured as $\tilde{\boldsymbol{\epsilon}} = \{u_{,x}\ u_{,y}\ v_{,x}\ v_{,y}\ w_{,x}\ w_{,y}\}^T$ for later derivations.

2.2. Theories based on Lagrange z-expansions with thickness stretching

Layerwise descriptions involving quasi-3D plate theories with transverse normal strains are necessary to take into account both discrete layer transverse shear effects and discrete layer thickness stretching effects [14,43]. This is attainable by considering, for example, that the through-thickness distributions of all displacement components are expressed resorting to one-dimensional Lagrange polynomials defined in each discrete layer thickness. As a result, the refinement of the displacement distributions is achieved by increasing the order of the Lagrange polynomials. In the present work, it is considered LW models involving quadratic and cubic Lagrange z-expansions, thus named LW Lag$N$ models, with $N = 2$ and 3, respectively. The first-order model ($N = 1$) is not considered due to the occurrence of thickness locking in displacement formulations with constant transverse normal strains and fully 3D stress–strain relations [14,35,36].

Considering that the displacements of each k-discrete layer are described by N-order Lagrange z-expansions, the displacement vector $\boldsymbol{u}^k = \{u^k\ v^k\ w^k\}^T$ is expressed as shown:

$$\boldsymbol{u}^k(x, y, z) = \sum_{j=1}^{N+1} \varphi_j^k(z) \boldsymbol{u}_j^k(x, y) \tag{8}$$

where $\varphi_j^k(z)$ are the one-dimensional Lagrange functions in the k-layer thickness at the j-node [35,36] and $\boldsymbol{u}_j^k = \{u_j^k \; v_j^k \; w_j^k\}^T$ is the corresponding displacement vector, i.e the nodal variables of the Lagrange z-expansions. The interlaminar continuity of displacements is imposed by assembling the displacement variables $\boldsymbol{u}_j^k$ at the interfaces between adjacent layers. In the particular case of three discrete layers, as intended in this work (Fig. 1), the through-thickness continuity of displacements implies that $\boldsymbol{u}_{N+1}^b = \boldsymbol{u}_1^c$ (bottom-core interface) and $\boldsymbol{u}_{N+1}^c = \boldsymbol{u}_1^t$ (core-top interface). Therefore, the assembled DOF of a LW Lag$N$ model can be structured as follows: $\boldsymbol{d} = \{\boldsymbol{u}_1^{b^T} \; \boldsymbol{u}_2^{b^T} \; \ldots \; \boldsymbol{u}_{N+1}^{b^T} \; \boldsymbol{u}_2^{c^T} \; \ldots \; \boldsymbol{u}_{N+1}^{c^T} \; \boldsymbol{u}_2^{t^T} \; \ldots \; \boldsymbol{u}_{N+1}^{t^T}\}^T$, which corresponds to a total of $(3N_L(N+1) - 3(N_L-1))$ independent DOF, where N_L stands for the number of discrete layers, i.e. $N_L = 3$.

Regarding the stress–strain relations, the proposed LW Lag$N$ models make use of 3D constitutive equations for each p-physical layer within each k-discrete layer, which are written in the global reference system as shown:

$$\begin{Bmatrix} \sigma_{xx}^{kp} \\ \sigma_{yy}^{kp} \\ \sigma_{zz}^{kp} \\ \sigma_{yz}^{kp} \\ \sigma_{xz}^{kp} \\ \sigma_{xy}^{kp} \end{Bmatrix} = \begin{bmatrix} \bar{C}_{11}^{kp} & \bar{C}_{12}^{kp} & \bar{C}_{13}^{kp} & 0 & 0 & \bar{C}_{16}^{kp} \\ \bar{C}_{12}^{kp} & \bar{C}_{22}^{kp} & \bar{C}_{23}^{kp} & 0 & 0 & \bar{C}_{26}^{kp} \\ \bar{C}_{13}^{kp} & \bar{C}_{23}^{kp} & \bar{C}_{33}^{kp} & 0 & 0 & \bar{C}_{36}^{kp} \\ 0 & 0 & 0 & \bar{C}_{44}^{kp} & \bar{C}_{45}^{kp} & 0 \\ 0 & 0 & 0 & \bar{C}_{45}^{kp} & \bar{C}_{55}^{kp} & 0 \\ \bar{C}_{16}^{kp} & \bar{C}_{26}^{kp} & \bar{C}_{36}^{kp} & 0 & 0 & \bar{C}_{66}^{kp} \end{bmatrix} \begin{Bmatrix} \varepsilon_{xx}^{kp} \\ \varepsilon_{yy}^{kp} \\ \varepsilon_{zz}^{kp} \\ \gamma_{yz}^{kp} \\ \gamma_{xz}^{kp} \\ \gamma_{xy}^{kp} \end{Bmatrix} \tag{9}$$

or using compact notation:

$$\boldsymbol{\sigma}^{kp} = \bar{\boldsymbol{C}}^{kp} \boldsymbol{\varepsilon}^{kp} \tag{10}$$

where $\bar{\boldsymbol{C}}^{kp}$ is the tensor of 3D elastic coefficients in the global reference system. In the case of composite layers with spatially varying fibre orientations $\theta(x,y)$ and temperature-dependent material properties, $\bar{\boldsymbol{C}}^{kp} = \bar{\boldsymbol{C}}^{kp}(x,y,\mathcal{T})$. The detailed expressions of the elastic coefficients as a function of the engineering material properties are available in [43]. Under the assumption of one-step thermal buckling analysis, the transverse normal thermal stresses σ_{zz}^{th} are neglected [20,46], and, therefore, the in-plane thermal stresses are derived resorting to the reduced plane stress constitutive relations stated in Eq. (6).

3. Aero-thermo-elastic FE formulation

The aero-thermo-elastic equilibrium equations of the multilayered panel are obtained using the Principle of Hamilton, which leads to the following variational formulation:

$$\sum_k \int_S \int_{h^k} \delta\boldsymbol{\varepsilon}^{k^T} \boldsymbol{\sigma}^k + \delta\tilde{\boldsymbol{\varepsilon}}^{k^T} \hat{\boldsymbol{\sigma}}_0^k \tilde{\boldsymbol{\varepsilon}}^k + \rho^k \delta\boldsymbol{u}^{k^T} \ddot{\boldsymbol{u}}^k \, dz dS = \int_S \delta\boldsymbol{u}^{t^T} |_{\frac{h}{2}} \boldsymbol{e}_z \Delta p \, dS \tag{11}$$

where δ stands for the variational operator and the double-dot for the second time derivative. Additionally, S, h^k and ρ^k are the in-plane surface, the thickness domain and the density of the k-discrete layer, respectively, with $k = \{t,c,b\}$, whereas $\boldsymbol{e}_z = \{0 \; 0 \; 1\}^T$. Regarding the loading conditions, $\hat{\boldsymbol{\sigma}}_0^k$ contains the applied thermal pre-stresses and Δp represents the distributed transverse load generated by the supersonic airflow on the upper surface ($z = h/2$).

Taking into account the structure of the generalized non-linear strains $\tilde{\boldsymbol{\varepsilon}}^k$, the k-layer initial thermal stresses $\hat{\boldsymbol{\sigma}}_0^k$ are deduced from Eq. (6) as shown:

$$\hat{\boldsymbol{\sigma}}_0^k = -\begin{bmatrix} \tilde{\boldsymbol{\beta}}^k & \boldsymbol{0} & \boldsymbol{0} \\ \boldsymbol{0} & \tilde{\boldsymbol{\beta}}^k & \boldsymbol{0} \\ \boldsymbol{0} & \boldsymbol{0} & \tilde{\boldsymbol{\beta}}^k \end{bmatrix} \Delta\mathcal{T} = \hat{\boldsymbol{\beta}}^k \Delta\mathcal{T} \tag{12}$$

where the auxiliary sub-matrices of stress-temperature coefficients $\tilde{\boldsymbol{\beta}}^k$ are given by:

$$\tilde{\boldsymbol{\beta}}^k = \begin{bmatrix} \bar{\beta}_{11}^k & \bar{\beta}_{12}^k \\ \bar{\beta}_{12}^k & \bar{\beta}_{22}^k \end{bmatrix} \tag{13}$$

The aerodynamic loading is described using the quasi-steady First-order Piston Theory, which is a simple and widely used aerodynamic model in the context of panel flutter analysis in the high supersonic regime, with Mach numbers ranging in $\sqrt{2} < M_\infty < 5$ [1,47]. Considering airflow along the x-axis, the resulting aerodynamic pressure distribution is the following:

$$\Delta p = -\lambda w_{,x}|_{\frac{h}{2}} - \mu \dot{w}|_{\frac{h}{2}} \tag{14}$$

such that the dynamic pressure parameter λ and aerodynamic damping parameter μ are related to the flight properties as shown:

$$\lambda = \frac{\rho_\infty a_\infty^2 M_\infty^2}{\sqrt{M_\infty^2 - 1}} \tag{15a}$$

$$\mu = \frac{\rho_\infty a_\infty M_\infty (M_\infty^2 - 2)}{(M_\infty^2 - 1)^{3/2}} \tag{15b}$$

where ρ_∞, a_∞ and $M_\infty = U_\infty / a_\infty$ represent the density, sound speed and freestream Mach number, respectively.

In Eq. (14), the steady-term reflects the influence of the curvature on the normal disturbance of the freestream, resulting in the aerodynamic stiffness, which is proportional to the dynamic pressure parameter λ. Moreover, the unsteady term is related to the transverse oscillations of the panel, providing the aerodynamic damping. Actually, the effect of the aerodynamic damping plays a minor stabilizing role on the occurrence of coupled-mode flutter, leading to slightly higher flutter boundaries [37,42,47]. As a result, the aerodynamic damping is disregarded in the present formulation, at this stage, which means that it is assumed $\mu = 0$ in latter derivations involving Eq. (14).

3.1. FE governing equations

To provide a concise derivation of the FE governing equations, the formulation is presented making use of a general notation with matrices and vectors, whose components are individually determined for each structural theory. Hence, the 1D z-expansions and 2D FE approximations of the displacements $\boldsymbol{u}^k$ and the strains $\boldsymbol{\varepsilon}^k$ and $\tilde{\boldsymbol{\varepsilon}}^k$, at the discrete layer level, are defined by:

$$\boldsymbol{u}^k = \boldsymbol{Z}^k \boldsymbol{N}^k \boldsymbol{d} \tag{16a}$$

$$\boldsymbol{\varepsilon}^k = \boldsymbol{S}^k \boldsymbol{B}^k \boldsymbol{d} \tag{16b}$$

$$\tilde{\boldsymbol{\varepsilon}}^k = \tilde{\boldsymbol{S}}^k \tilde{\boldsymbol{B}}^k \boldsymbol{d} \tag{16c}$$

where $\boldsymbol{Z}^k$, $\boldsymbol{S}^k$ and $\tilde{\boldsymbol{S}}^k$ contain the z-expansion functions and their derivatives in the thickness direction, while $\boldsymbol{N}^k$, $\boldsymbol{B}^k$ and $\tilde{\boldsymbol{B}}^k$ establish the necessary FE approximations in-plane via 2D shape functions. More precisely, the applied 2D shape functions are quadratic Lagrange functions, which constitute the basis for the nine-node quadrilateral element (Q9) [43]. Therefore, the element DOF are structured as $\boldsymbol{d} = \{\boldsymbol{d}_1^T \; \ldots \; \boldsymbol{d}_9^T\}^T$, where $\boldsymbol{d}_i$ stands for the element nodal DOF. In the particular case of ESL descriptions, the expansion matrices in Eq. (16) are independent of the index k, since only one discrete layer is applied to describe the whole multilayered panel.

Considering the variational principle stated in Eq. (11) along with the FE approximations defined in Eq. (16), the stress–strain relations in Eq. (10), as well as the external loads in Eqs. (14) and (12), the FE equilibrium equations arise as follows:

$$\boldsymbol{M}\ddot{\boldsymbol{d}} + (\boldsymbol{K} + \lambda \boldsymbol{K}_a + \Delta\mathcal{T} \boldsymbol{K}_g)\boldsymbol{d} = \boldsymbol{0} \tag{17}$$

where $\boldsymbol{M}$, $\boldsymbol{K}$, $\boldsymbol{K}_a$ and $\boldsymbol{K}_g$ are the mass matrix, the purely elastic stiffness matrix, the aerodynamic stiffness matrix and the geometric stiffness matrix, respectively.

Since each k-discrete layer can represent, in general, a sublaminate with a total of N_p^k physical layers, the implied FE matrices are thus conveniently derived as shown:

$$\boldsymbol{M} = \sum_k \sum_{p=1}^{N_p^k} \int_\Omega \boldsymbol{N}^{k^T} \left(\int_{h^{kp}} \rho^{kp} \boldsymbol{Z}^{k^T} \boldsymbol{Z}^k dz \right) \boldsymbol{N}^k d\Omega \tag{18a}$$

$$\boldsymbol{K} = \sum_{k} \sum_{p=1}^{N_p^k} \int_{\Omega} \boldsymbol{B}^{k^T} \left(\int_{h^{kp}} \boldsymbol{S}^{k^T} \bar{\boldsymbol{C}}^{kp} \boldsymbol{S}^k dz \right) \boldsymbol{B}^k d\Omega \tag{18b}$$

$$\boldsymbol{K}_g = \sum_{k} \sum_{p=1}^{N_p^k} \int_{\Omega} \tilde{\boldsymbol{B}}^{k^T} \left(\int_{h^{kp}} \tilde{\boldsymbol{S}}^{k^T} \hat{\boldsymbol{\beta}}^{kp} \tilde{\boldsymbol{S}}^k dz \right) \tilde{\boldsymbol{B}}^k d\Omega \tag{18c}$$

$$\boldsymbol{K}_a = \int_{\Omega} \boldsymbol{N}^{t^T} \boldsymbol{Z}^{t^T} |_{\frac{h}{2}} \boldsymbol{e}_z \boldsymbol{e}_z^T \boldsymbol{Z}^t |_{\frac{h}{2}} \boldsymbol{N}_{,x}^t d\Omega \tag{18d}$$

where the integrals in each thickness domain h^{kp} are evaluated using exact integration, whereas the integration on the FE domain Ω is performed numerically by means of Gauss quadrature, with reduced integration for the shear terms of the stiffness matrix (Eq. (18b)) to avoid shear locking [43]. Furthermore, it is worth highlighting that: (i) for models based on shear deformation theories devoid of thickness stretching, the $\bar{\boldsymbol{C}}^{kp}$ tensor in Eq. (18b) must be replaced by $\bar{\boldsymbol{Q}}^{kp}$, in agreement with the reduced plane stress equations stated in Eq. (4); (ii) the fibre orientations of composite layers with curvilinear fibres are evaluated at each integration point; and (iii) the material-dependent FE matrices are contingent on the applied temperature when dealing with temperature-dependent material properties, i.e. $\boldsymbol{M} = \boldsymbol{M}(\mathcal{T})$, $\boldsymbol{K} = \boldsymbol{K}(\mathcal{T})$ and $\boldsymbol{K}_g = \boldsymbol{K}_g(\mathcal{T})$, with $\mathcal{T} = \mathcal{T}_0 + \Delta\mathcal{T}$.

3.2. Flutter and buckling problems

After the standard FE assemblage and imposition of boundary conditions, the characteristic equation of the global eigenvalue problem is written as follows:

$$\left| \left(\boldsymbol{K} + \lambda \boldsymbol{K}_a + \Delta\mathcal{T} \boldsymbol{K}_g \right) + s_n^2 \boldsymbol{M} \right| = 0 \tag{19}$$

where $s_n^2 = -\omega_n^2(1 + ig_n)$, with $i = \sqrt{-1}$, is the complex eigenvalue associated to the n-mode of vibration, which allows for the evaluation of the natural frequency (ω_n) and modal loss factor (g_n). The free vibration analysis in vacuum, without thermal loads, corresponds to the particular case of $\lambda = 0$ Pa and $\Delta\mathcal{T} = 0$ K, such that $s_n^2 = -\omega_n^2$.

- *Linear flutter analysis*:

Regarding linear aeroelastic flutter analysis, with or without thermal loads, the goal is to find the lowest value of pressure parameter λ that promotes the occurrence of a dynamically unstable mode, with negative modal loss factor $g_n < 0$, in the solution of Eq. (19). Hence, for a given temperature difference $\Delta\mathcal{T}$, the critical flutter pressure parameter λ_F is estimated using the same direct iterative procedure on λ from the authors previous works, as carefully detailed in Moreira et al. [35,36]. This standard approach involves progressively increasing λ until the onset of flutter instability is detected via mode coalescence. The flutter boundary can also be expressed in terms of the critical Mach number M_{cr} at a designated flight altitude, which defines the atmospheric properties involved in Eq. (15).

Under the assumption of null aerodynamic damping, all modes show zero modal loss factor prior to flutter and mode coalescence is explicitly verified as flutter occurs [36,42,47], i.e. the occurrence of flutter is detectable by the perfect coalescence of two natural frequencies. The natural frequency at which the two modes involved in flutter come together is herein defined as the flutter frequency $f_F = \omega_F/(2\pi)$.

- *Linearized thermal buckling analysis*:

Assuming stable pre-buckling behaviour, the linearized thermal buckling analysis is recovered by neglecting the aerodynamic loads as well as the inertial terms in Eq. (19). Therefore, the critical temperature difference $\Delta\mathcal{T}_{\text{cr}}$ that leads to buckling instability corresponds to the lowest eigenvalue solution of the following characteristic equation:

$$\left| \boldsymbol{K} + \Delta\mathcal{T}_{\text{cr}} \boldsymbol{K}_g \right| = 0 \tag{20}$$

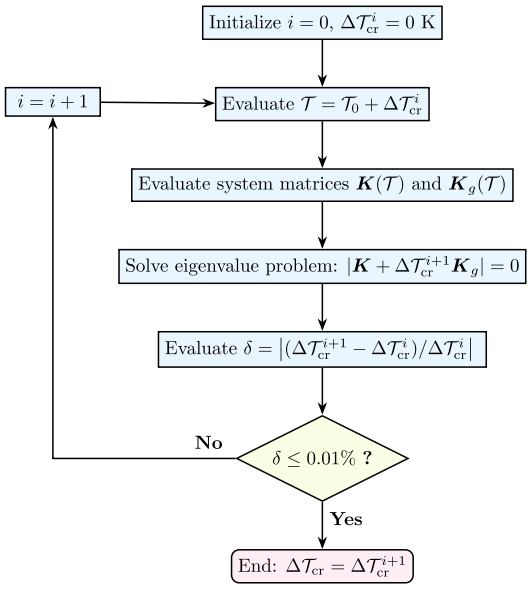

Fig. 3. Flowchart of the linearized thermal buckling analysis with temperature-dependent material properties.

It is important to emphasize that in the case of temperature-dependent material properties, where $\boldsymbol{K} = \boldsymbol{K}(\mathcal{T})$ and $\boldsymbol{K}_g = \boldsymbol{K}_g(\mathcal{T})$, an iterative procedure is necessary to obtain the critical temperature difference [10]. The corresponding flowchart is presented in Fig. 3 and it is briefly described as follows:

1. Initialize iteration counter $i = 0$ and initial guess $\Delta\mathcal{T}_{\text{cr}}^i = 0$ K, and define the reference temperature $\mathcal{T}_0$ (in the present numerical applications $\mathcal{T}_0 = 300$ K);
2. Compute current temperature $\mathcal{T} = \mathcal{T}_0 + \Delta\mathcal{T}_{\text{cr}}^i$, evaluate the material properties and the necessary FE matrices at the current temperature, and then solve the eigenvalue problem stated in Eq. (20) to obtain the new critical temperature difference $\Delta\mathcal{T}_{\text{cr}}^{i+1}$;
3. Compute the relative difference between two subsequent solutions $\delta = \left|(\Delta\mathcal{T}_{\text{cr}}^{i+1} - \Delta\mathcal{T}_{\text{cr}}^i)/\Delta\mathcal{T}_{\text{cr}}^i\right|$ and verify the convergence: if $\delta \leq 0.01\%$, accept $\Delta\mathcal{T}_{\text{cr}} = \Delta\mathcal{T}_{\text{cr}}^{i+1}$ and terminate; otherwise, increment i and repeat the previous step.

4. Numerical applications

The numerical applications are structured in three parts: (i) Section 4.1 provides the validation of the proposed FE models by comparison with available literature solutions regarding the linearized thermal buckling analysis of composite laminates with curvilinear fibres and temperature-dependent material properties; (ii) Section 4.2 focuses on the linear aero-thermo-elastic flutter and buckling stability analysis of supersonic laminated composite panels, with either unidirectional or curvilinear fibres, evaluating the impact of the temperature-dependent material properties on the solutions; and (iii) Section 4.3 extends the preceding analyses for the case of soft core sandwich panels.

In the numerical applications that follow, the boundary conditions explored are either simply supported or clamped constraints on all sides of the panel, which are the most common and meaningful boundary conditions in supersonic panel flutter analysis using the classical quasi-steady First-order Piston Theory [1,47]. To be clear, the simply supported boundary conditions are the following:

$$u = w = 0 \text{ at } y = 0, b \tag{21a}$$

$$v = w = 0 \text{ at } x = 0, a \tag{21b}$$

whereas for clamped panels, the three displacement components are constrained in all four edges.

The flutter pressure parameters are provided in the following nondimensionalized form:

$$\tilde{\lambda}_F = \frac{\lambda_F}{G_0}\left(\frac{a}{h}\right)^3 \tag{22}$$

where a/h is the side-to-thickness ratio of the panel and $G_0 = 6$ GPa is the shear modulus G_{12} of the composite material at the initial reference temperature.

4.1. Validation

The present models are validated by comparison with the solutions reported by Li and Nie [10] regarding the linearized thermal buckling analysis of simply supported VSC plates with linearly varying temperature-dependent material properties. The square panels have sides $a = b = 1$ m and a side-to-thickness ratio of $a/h = 30$, being composed by twenty layers of equal thickness. Three symmetric stacking sequences are considered: $(\pm 45)_{5s}$, $(\pm\langle 0, 15\rangle)_{5s}$ and $(\pm\langle 30, 60\rangle)_{5s}$. The implied temperature-dependent (TD) material properties are given as shown:

$$E_1 = E_1^0(1 + \tilde{E}_1\Delta\mathcal{T}),\ E_2 = E_3 = E_2^0(1 + \tilde{E}_2\Delta\mathcal{T}) \tag{23a}$$

$$G_{12} = G_{13} = G_{12}^0(1 + \tilde{G}_{12}\Delta\mathcal{T}),\ G_{23} = G_{23}^0(1 + \tilde{G}_{23}\Delta\mathcal{T}) \tag{23b}$$

$$\alpha_{11} = \alpha_{11}^0(1 + \tilde{\alpha}_{11}\Delta\mathcal{T}),\ \alpha_{22} = \alpha_{33} = \alpha_{22}^0(1 + \tilde{\alpha}_{22}\Delta\mathcal{T}) \tag{23c}$$

$$\nu_{12} = \nu_{13} = \nu_{23} = \nu_0 \tag{23d}$$

where $E_1^0/E_2^0 = 40$, $G_{12}^0/E_2^0 = G_{13}^0/E_2^0 = 0.5$, $G_{23}^0/E_2^0 = 0.2$, $\nu_0 = 0.25$, $\alpha_{11}^0 = 10^{-6}$/K, $\alpha_{22}^0 = 10^{-5}$/K, $\tilde{E}_1 = -0.5 \times 10^{-3}$, $\tilde{E}_2 = \tilde{G}_{12} = \tilde{G}_{13} = \tilde{G}_{23} = -0.2 \times 10^{-3}$ and $\tilde{\alpha}_{11} = \tilde{\alpha}_{22} = 0.5 \times 10^{-3}$. The temperature-independent (TID) material properties are estimated at the initial reference temperature, which means that it is assumed $\Delta\mathcal{T} = 0$ K in Eq. (23).

Table 1 presents the critical temperature differences predicted by the proposed structural models alongside the ESL FSDT solutions reported by Li and Nie [10]. The present models solutions are obtained using a mesh with 10 × 10 Q9 elements. As regards to the LW models, six material layers are considered in the top and bottom discrete layers, while the remaining eight layers are described by the middle/core discrete layer. The present solutions are in good agreement with the reference solutions, thus validating the proposed models for linearized thermal buckling analysis of VSC laminates with temperature-dependent material properties. Nonetheless, it is worth mentioning that the high-order LW models predict slightly lower temperature differences due to the low value of side-to-thickness ratio, which corresponds, in fact, to a moderately thick panel.

Regarding free vibration and supersonic aeroelastic flutter analysis, a complete validation with available literature solutions is presented in previous works by the authors [35–37,39], including both VSC laminates and soft core sandwich panels (with temperature-independent material properties).

4.2. Laminated composite panels

This subsection is focused on the linear aero-thermo-elastic flutter and buckling stability of symmetric laminated composite panels, with either unidirectional or curvilinear fibres. The test cases are based on the examples of four-layer composite panels $(\pm\langle\theta_0, \theta_1\rangle)_s$ investigated by Li and Nie [10] concerning thermal buckling analysis. Accordingly, the panels in-plane dimensions are $a = b = 1$ m and the side-to-thickness ratio is $a/h = 100$ (equal thickness composite layers). In terms of LW modelling, the two inner layers $(\langle\text{-}\theta_0, \text{-}\theta_1\rangle)_2$ are conveniently treated as a sublaminate, using an ESL description, i.e. the middle discrete layer in Fig. 1 represents two physical layers.

Table 1
Critical temperature differences $\Delta\mathcal{T}_{cr} \times 10^{-3}$ (K) of simply supported composite panels ($a/h = 30$): comparison with available literature solutions.

Model	$(\pm 45)_{5s}$		$(\pm\langle 0, 15\rangle)_{5s}$		$(\pm\langle 30, 60\rangle)_{5s}$	
	$\Delta\mathcal{T}_{cr}$ [a]	$\Delta\mathcal{T}_{cr}$ [b]	$\Delta\mathcal{T}_{cr}$ [a]	$\Delta\mathcal{T}_{cr}$ [b]	$\Delta\mathcal{T}_{cr}$ [a]	$\Delta\mathcal{T}_{cr}$ [b]
ESL FSDT [10]	1.247	0.834	0.785	0.590	1.348	0.865
ESL FSDT	1.246	0.833	0.785	0.590	1.348	0.865
ESL TSDT	1.242	0.832	0.784	0.589	1.345	0.864
LW FSDT	1.242	0.832	0.784	0.589	1.345	0.864
LW TSDT	1.235	0.829	0.783	0.589	1.339	0.862
LW Lag2	1.236	0.830	0.783	0.588	1.338	0.860
LW Lag3	1.234	0.829	0.782	0.587	1.337	0.859

[a] TID; [b] TD.

Table 2
Temperature-dependent properties of the graphite-epoxy material [10].

Elastic Moduli (GPa)	Temperature $\mathcal{T}$ (K)					
	300	325	350	375	400	425
E_1	130	130	130	130	130	130
$E_2 = E_3$	9.50	8.50	8.00	7.50	7.00	6.75
$G_{12} = G_{13} = 2G_{23}$	6.00	6.00	5.50	5.00	4.75	4.50

The mechanical properties of the graphite-epoxy composite material are interpolated using the data given in Table 2, for a temperature range between 300 K and 425 K, as illustrated in Fig. 4. In line with Li and Nie [10], the temperature-dependent Young and shear moduli are approximated by the following functions:

$$E_2 = E_3 = P_{-1}^E/\mathcal{T} + P_0^E + P_1^E\mathcal{T} + P_2^E\mathcal{T}^2 + P_3^E\mathcal{T}^3 \tag{24a}$$

$$G_{12} = G_{13} = 2G_{23} = P_{-1}^G/\mathcal{T} + P_0^G + P_1^G\mathcal{T} + P_2^G\mathcal{T}^2 + P_3^G\mathcal{T}^3 \tag{24b}$$

The Poisson coefficients ($\nu_{12} = \nu_{13} = \nu_{23} = 0.3$), the thermal expansion coefficients ($\alpha_{11} = -0.3 \times 10^{-6}$ /K and $\alpha_{22} = \alpha_{33} = 28.1 \times 10^{-6}$ /K) and the density ($\rho = 1600$ kg/m^3) are assumed temperature-independent. This simplified set of temperature-dependent material properties is denoted, in short, by TD_1. When considering temperature-independent (TID) material properties, the Young and shear moduli are estimated at the initial reference temperature $\mathcal{T}_0 = 300$ K.

In real applications, the thermal expansion coefficients of graphite-epoxy composites tend to increase with the temperature [23]. To include temperature-dependent thermal expansion coefficients, two additional sets of temperature-dependent material properties are explored assuming linear variations of these properties, as in the example of Section 4.1, which are given by:

$$\alpha_{11} = -0.3 \times 10^{-6}(1 + \tilde{\alpha}_{11}\Delta\mathcal{T}) \tag{25a}$$

$$\alpha_{22} = \alpha_{33} = 28.1 \times 10^{-6}(1 + \tilde{\alpha}_{22}\Delta\mathcal{T}) \tag{25b}$$

where $\tilde{\alpha}_{22} = -\tilde{\alpha}_{11} = 0.5 \times 10^{-3}$ /K^2 and $\tilde{\alpha}_{22} = -\tilde{\alpha}_{11} = 0.5 \times 10^{-2}$ /K^2 in the TD_2 and TD_3 material properties, respectively. In sum, four sets of material properties are explored, viz. TID, TD_1, TD_2 and TD_3 material properties.

The convergence study is presented in Table 3, considering the LW Lag3 model for the analysis of the $(\pm\langle 0, 45\rangle)_s$ laminated panel, with either SSSS or CCCC boundary conditions (BC). In more detail, the numerical results include the free vibration and flutter solutions without thermal loads, as well as the thermal buckling solutions with and without temperature-dependent properties. For both boundary conditions, flutter occurs due to the coalescence of the first two modes. To ensure converged solutions, regardless of the boundary conditions, the mesh with 14 × 14 Q9 elements is considered in the following numerical analyses. Even though not shown, for brevity, a similar convergence behaviour is observed when making use of the remaining structural theories explored in this work. Additionally, it is worth mentioning that the convergence of the mode shapes is also attained by the selected mesh.

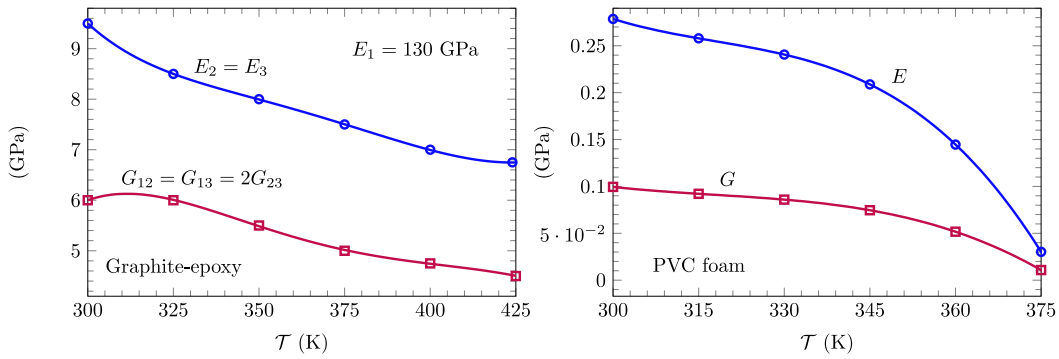

Fig. 4. Variation of the Young and shear moduli with the temperature: graphite-epoxy (on the left) and PVC foam (on the right).

Table 3
Convergence analysis results of the LW Lag3 model considering the $(\pm\langle 0, 45\rangle)_s$ composite panel: first five natural frequencies f_n (Hz), critical temperature differences $\Delta\mathcal{T}_{cr}$ (K), nondimensionalized flutter pressure parameters $\tilde{\lambda}_F$ and flutter frequencies f_F (Hz).

BC	Mesh	f_1	f_2	f_3	f_4	f_5	$\Delta\mathcal{T}_{cr}$ [a]	$\Delta\mathcal{T}_{cr}$ [b]	$\Delta\mathcal{T}_{cr}$ [c]	$\tilde{\lambda}_F$	f_F
SSSS	6 × 6	53.33	92.16	152.01	155.42	201.52	48.64	55.27	43.81	388.3	102.06
	8 × 8	53.27	91.99	151.20	155.04	200.85	48.50	55.08	43.69	387.9	102.07
	10 × 10	53.24	91.92	150.96	154.90	200.59	48.43	54.98	43.63	387.7	102.04
	12 × 12	53.22	91.88	150.86	154.83	200.46	48.39	54.92	43.59	387.6	102.02
	14 × 14	53.20	91.85	150.82	154.79	200.38	48.36	54.88	43.57	387.6	102.02
CCCC	6 × 6	85.14	126.10	194.02	217.67	260.09	75.42	88.78	63.28	617.8	144.08
	8 × 8	84.93	125.62	191.83	216.06	258.13	74.80	87.86	62.83	612.6	143.73
	10 × 10	84.85	125.44	191.16	215.57	257.51	74.59	87.57	62.68	610.9	143.59
	12 × 12	84.81	125.35	190.87	215.36	257.25	74.51	87.45	62.62	610.2	143.52
	14 × 14	84.78	125.30	190.71	215.26	257.11	74.46	87.39	62.59	609.8	143.48

[a] TID; [b] TD_1; [c] TD_3.

The impact of the temperature-dependent material properties on the critical temperature is illustrated in Fig. 5, considering simply supported composite panels with either unidirectional fibres $(\pm\theta)_s$, where $0° \leq \theta \leq 90°$, or curvilinear fibres $(\pm\langle\theta_0, \theta_1\rangle)_s$, where $\theta_0 = \{0°, 45°, 60°\}$ and $0° \leq \theta_1 \leq 90°$. The highest discrepancies between the TD material properties and the TID material properties are annotated in Fig. 5 for comparison purposes. For the TID and TD_1 material properties, it is worth emphasizing that the presents result are in agreement with the solutions reported by Li and Nie [10], where similar figures can be found regarding these two sets of material properties.

Comparing the trends provided in Fig. 5, it is perceived that the TD_1 material properties lead to higher critical temperature differences than the TID material properties. This is explained by the fact that the thermal stresses depended not only on the elastic coefficients, but also on the thermal expansions coefficients (Eq. (6)), which are assumed constant in the TD_1 material properties. Since the elastic coefficients decrease with the applied temperature, while the thermal expansion coefficients are treated as temperature-independent, the critical stress state is reached at a higher temperature when comparing the TD_1 material properties to the TID material properties. The same conclusions holds equally for TD_2 material properties because the growing rate of the thermal expansion coefficients with the temperature is very subtle. However, when considering the TD_3 material properties, the decreasing elastic coefficients along with the increasing thermal expansion coefficients result in lower critical temperatures as compared to the TID material properties, i.e. $\Delta\mathcal{T}_{cr}^{TD_3} < \Delta\mathcal{T}_{cr}^{TID} < \Delta\mathcal{T}_{cr}^{TD_2} < \Delta\mathcal{T}_{cr}^{TD_1}$. Hence, a careful assessment of the temperature-dependency associated to the thermal expansion coefficients is essential to accurately estimate the critical temperatures.

From a design perspective, the parametric results presented in Fig. 5 confirm that, among unidirectional fibre laminates $(\pm\theta)_s$, the highest thermal buckling resistance is achieved for $\theta = 45°$. Similarly, among the various VSC laminates $(\pm\langle\theta_0, \theta_1\rangle)_s$, the highest thermal buckling temperature is achieved for $\theta_0 = 60°$ and $\theta_1 = 30°$, surpassing the previously mentioned configuration with unidirectional fibres at ±45°. These two configurations fully agree with the original benchmark proposed by Li and Nie [10] and are closely aligned with optimal designs obtained through formal optimization by Zhao et al. [24]. The superior performance of the variable stiffness configuration arises from the ability of the curvilinear fibre paths to favourably redistribute in-plane compressive thermal stresses. In particular, the reduced fibre angle (±30°) near the left- and right-boundaries enhances local axial stiffness along the x-direction, while the higher central angle (±60°) primarily favours axial stiffness along the y-direction, creating a beneficial stiffness gradient that delays the onset of buckling instability. Therefore, it is emphasized that VSC laminates with curvilinear fibres can outperform conventional composite laminates with unidirectional fibres in thermal buckling resistance.

The $(\pm45)_s$ and $(\pm\langle 60, 30\rangle)_s$ laminated composite panels are selected for in-depth analysis in the subsequent figures, as these represent the most thermally robust designs and allow meaningful assessment of modelling accuracy under demanding conditions. An introduction to the aero-thermo-elastic flutter analysis is provided in Fig. 6, taking the $(\pm\langle 60, 30\rangle)_s$ composite panel as an example. For increasing temperature differences, Fig. 6 shows the variation of the first four natural frequencies with the nondimensionalized flutter pressure parameter, considering both TID and TD_3 material properties. In spite of the applied temperature, flutter occurs due to the aeroelastic coupling of the first two modes, which is marked by the coalescence of the corresponding natural frequencies at the critical flutter pressure parameter. Note that in the absence of thermal loads, i.e. for $\Delta\mathcal{T} = 0$ K, the solutions coincide because the TID material properties are estimated at the initial reference temperature.

A comparative analysis of the trends provided in Fig. 6 indicates that the natural frequencies and nondimensionalized flutter pressure parameter decrease with the temperature. In addition, when considering the TD_3 material properties, the natural frequencies and flutter boundaries are lower as compared to those derived assuming the TID

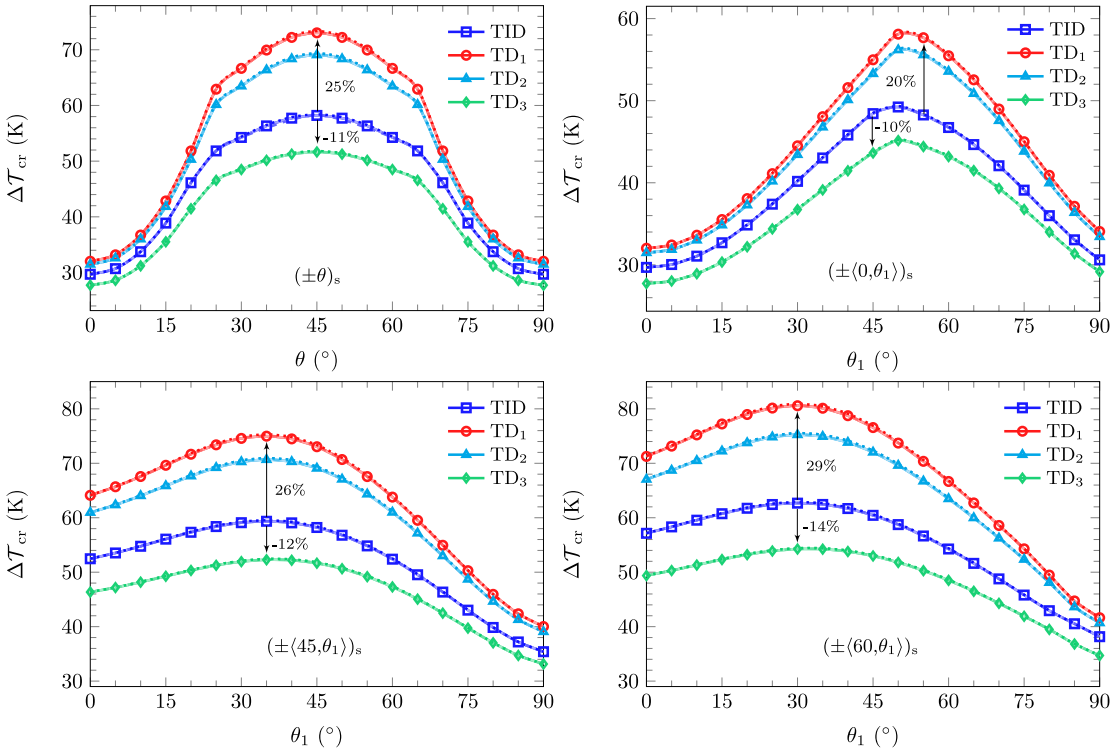

Fig. 5. Critical temperature differences $\Delta\mathcal{T}_{cr}$ of simply supported composite panels with unidirectional and curvilinear fibres: ESL FSDT (dotted lines), ESL TSDT (dashed lines) and LW Lag3 model (solid lines).

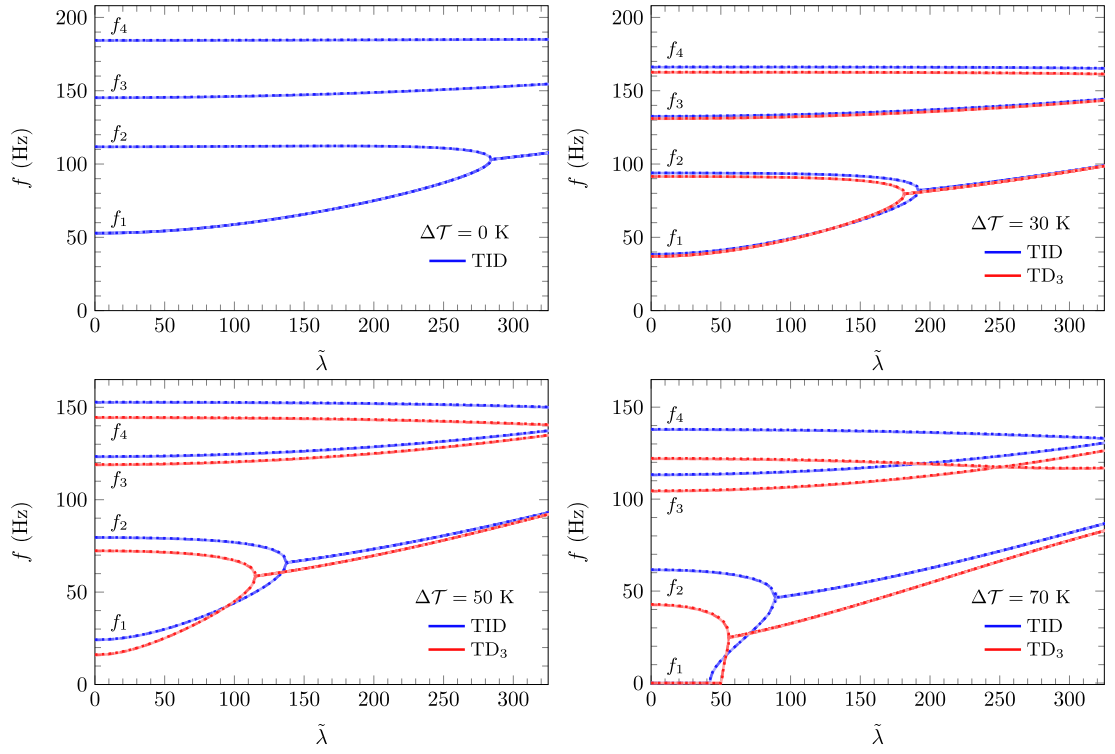

Fig. 6. Evolution of the first four natural frequencies f_n with the nondimensionalized pressure parameter $\tilde{\lambda}$ of the simply supported $(\pm\langle 60, 30\rangle)_s$ composite panel, under increasing temperature differences $\Delta\mathcal{T}$: ESL FSDT (dotted lines), ESL TSDT (dashed lines) and LW Lag3 (solid lines) models.

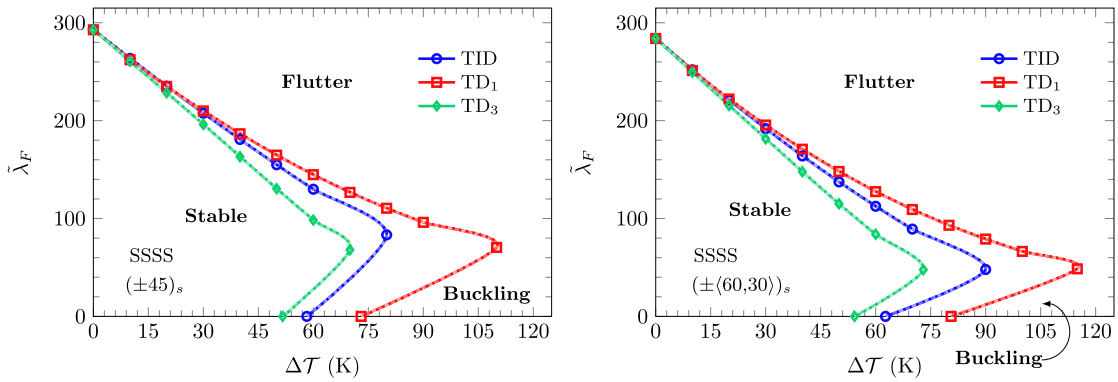

Fig. 7. Evolution of the nondimensionalized flutter pressure parameter $\tilde{\lambda}_F$ with the applied temperature difference $\Delta\mathcal{T}$ of simply supported composite panels: ESL FSDT (dotted lines), ESL TSDT (dashed lines) and LW Lag3 (solid lines) models.

material properties. More precisely, for $\Delta\mathcal{T} = 70$ K, the critical buckling temperature is exceeded, giving rise to a zero frequency condition at low nondimensionalized pressure parameters, which means that the panel is statically unstable under such external conditions. As the nondimensionalized pressure parameter increases, the static buckling instability ceases and only then flutter occurs.

Considering the $(\pm 45)_s$ and $(\pm\langle 60, 30\rangle)_s$ laminated composite panels, Fig. 7 presents the evolution of the nondimensionalized flutter pressure parameter with the applied temperature difference, considering the TID, TD_1 and TD_3 material properties. In more detail, the flutter pressure parameter decreases with the temperature until flutter starts to occur immediately after the disappearance of buckling, as carefully illustrated in Fig. 6 when considering $\Delta\mathcal{T} = 70$ K and TD_3 material properties.

Additionally, Fig. 7 shows that when the temperature-dependency of the thermal expansion coefficients is included, as in the TD_3 material properties, the resulting flutter pressure parameters and critical temperature differences are lower in comparison to the TID and TD_1 material properties. Therefore, the stable region where the panel can operate without experiencing flutter and buckling instabilities is significantly reduced by the temperature-dependency of the material properties. It is important to note that since the TD_1 material properties include solely the temperature dependency of the elastic coefficients, while maintaining constant thermal expansion coefficients, the flutter pressure parameters are overestimated as compared to the case with TID material properties.

In summary, the temperature rise degrades the flutter resistance of laminated composite panels through two synergistic mechanisms: (i) temperature-dependent material properties cause thermal softening of the composite material (reduced elastic moduli), especially due to the polymeric nature of the matrix material, lowering overall structural stiffness and natural frequencies; and (ii) thermal loads generate in-plane compressive stresses that introduce geometric stiffness reduction, shifting the panel toward buckling and bringing vibrational modes into coalescence under lower dynamic pressure parameters.

Regarding the models accuracy assessment, Figs. 5, 6 and 7 show a fairly good agreement between the ESL FSDT and ESL TSDT models and the LW Lag3 model, mostly because it is considered thin panels. To provide further insight into the role of the structural theories, detailed numerical results are provided in Table 4, considering the $(\pm 45)_s$ and $(\pm\langle 60, 30\rangle)_s$ laminated composite panels, with either TID or TD_3 material properties. It is worth emphasizing that: (i) the flutter pressure parameters summarized in Table 4 are all related to the coalescence of the first two modes, as shown in part by Fig. 6; and (ii) in the absence of thermal loads, i.e. for $\Delta\mathcal{T} = 0$ K, the flutter boundaries coincide for both TID and TD material properties.

A careful examination of the thermal buckling solutions presented in Table 4 reveals that the selected stacking sequences and temperature-dependent material properties do not affect the discrepancies between the ESL and LW models. For example, in both laminates, the simpler model investigated in this work (ESL FSDT) predicts 0.5% higher critical temperatures than the most refined model (LW Lag3) when considering either TID or TD_3 material properties. However, in the context of aero-thermo-elastic flutter analysis, it is observed that the differences among structural models are more pronounced when addressing temperature-dependent material properties and curvilinear fibres. As the temperature increases, it is also observed a greater divergence between the TID and TD_3 material properties, as well as among the flutter estimations of the structural models. More precisely, in the flutter analysis of the $(\pm\langle 60, 30\rangle)_s$ composite panel without applied thermal loads, the discrepancy between the ESL FSDT model and the LW Lag3 model is approximately 0.3%. However, when the temperature increase reaches $\Delta\mathcal{T} = 70$ K, the corresponding discrepancy rises to 0.7% and 1.6% for the TID and TD_3 material properties, respectively.

It is important to highlight that by considering models with high-order kinematics, such as the ESL TSDT, LW TSDT and LW Lag2 models, the flutter solutions are closer to the LW Lag3 model. This is explained by the fact that the 3D mechanical response of highly anisotropic composite laminates under in-plane thermal loads and transverse aerodynamic loads can be quite complicated, encompassing bending, membrane and shear deformations, all together, which can only be properly captured by high-order models. Nonetheless, since thin panels are concerned, the ESL TSDT, LW FSDT and LW TSDT models are capable of providing fairly accurate solutions, even without including thickness stretching effects.

Considering the $(\pm\langle 60, 30\rangle)_s$ composite laminate under simply supported boundary conditions, Fig. 8 presents the evolution of the critical flutter Mach number M_{cr} with the flight altitude H. The solutions are obtained resorting the LW Lag3 model, whereas the atmospheric properties are derived in accordance with the International Standard Atmosphere (ISA). Moreover, the Mach number range where the First-order Piston Theory is valid, i.e. $\sqrt{2} < M_\infty < 5$, is indicated using two subtle horizontal lines. In addition to the original case with $a/h = 100$, it is also considered a thinner panel with the same in-plane dimensions and $a/h = 125$. The critical temperature differences of the new panel with $a/h = 125$ are approximately $\Delta\mathcal{T}_{cr} = 40$ K and 37 K when considering the TID and TD_3 material properties, respectively, which are lower than the corresponding values for $a/h = 100$, namely 63 and 54 K.

In the absence of thermal loads ($\Delta\mathcal{T} = 0$ K), Fig. 8 reveals that none of the panels experiences flutter in the supersonic range since $M_{cr} > 5$. However, as the applied temperature increases, the critical Mach numbers decrease, such that supersonic panel flutter starts to be verified. For $a/h = 100$, the occurrence of supersonic flutter is noticeable when the applied temperature difference is $\Delta\mathcal{T} = 70$ K, which is a value above the critical temperature difference. For this temperature difference, the inclusion of TD_3 material properties significantly lowers the critical Mach numbers. More specifically, it is verified that for

Table 4
Critical temperature differences $\Delta\mathcal{T}_{cr}$ (K) and nondimensionalized flutter pressure parameters $\tilde{\lambda}_F$ of simply supported composite panels under uniform temperature rise.

		$\tilde{\lambda}=0$		$\Delta\mathcal{T}=0$ K	$\Delta\mathcal{T}=30$ K		$\Delta\mathcal{T}=50$ K		$\Delta\mathcal{T}=70$ K	
Case	Model	$\Delta\mathcal{T}_{cr}$ [a]	$\Delta\mathcal{T}_{cr}$ [b]	$\tilde{\lambda}_F$ [a,b]	$\tilde{\lambda}_F$ [a]	$\tilde{\lambda}_F$ [b]	$\tilde{\lambda}_F$ [a]	$\tilde{\lambda}_F$ [b]	$\tilde{\lambda}_F$ [a]	$\tilde{\lambda}_F$ [b]
$(\pm45)_s$	ESL FSDT	58.40	51.80	293.3	208.0	196.5	155.3	130.8	106.4	68.4
	ESL TSDT	58.26	51.68	292.9	207.6	196.1	154.9	130.4	106.1	68.1
	LW FSDT	58.23	51.65	292.8	207.6	196.1	154.9	130.4	106.1	68.0
	LW TSDT	58.09	51.52	292.4	207.2	195.7	154.5	130.1	105.8	67.7
	LW Lag2	58.21	51.63	292.8	207.6	196.1	154.9	130.4	106.1	68.1
	LW Lag3	58.12	51.54	292.5	207.3	195.8	154.7	130.2	105.9	67.8
$(\pm\langle60,30\rangle)_s$	ESL FSDT	62.87	54.39	284.4	192.3	182.0	137.8	115.4	89.6	56.2
	ESL TSDT	62.74	54.28	284.0	191.9	181.6	137.4	115.0	89.2	55.6
	LW FSDT	62.71	54.25	283.9	191.8	181.5	137.4	115.0	89.2	55.6
	LW TSDT	62.56	54.12	283.5	191.5	181.2	137.1	114.6	88.9	55.3
	LW Lag2	62.68	54.23	283.8	191.8	181.5	137.4	114.9	89.2	55.6
	LW Lag3	62.58	54.14	283.6	191.5	181.3	137.1	114.7	89.0	55.3

[a] TID; [b] TD_3.

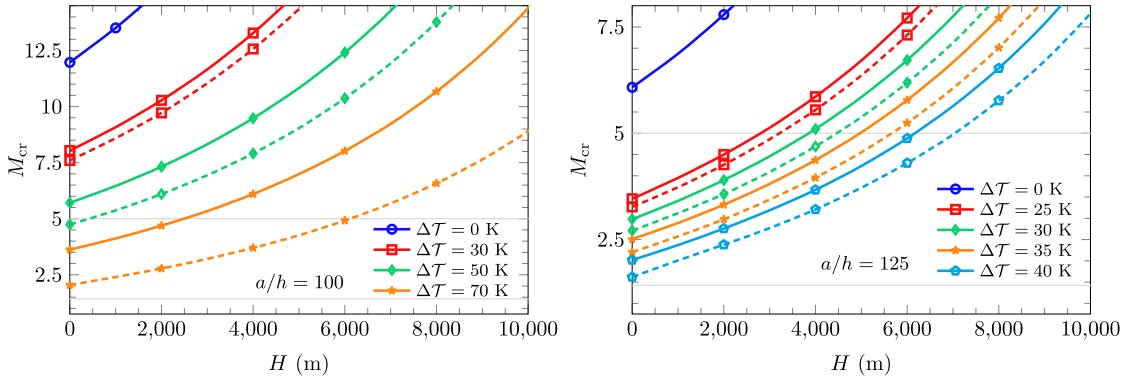

Fig. 8. Evolution of the critical flutter Mach number M_{cr} with the altitude H of the simply supported $(\pm\langle60,30\rangle)_s$ composite panel with $a/h = 100$ and 125, under increasing temperature differences $\Delta\mathcal{T}$: TID (solid lines) and TD_3 (dashed lines) material properties.

$\Delta\mathcal{T} = 70$ K, the panel can safely fly at Mach number $M_\infty = 3$ (for example) when considering the TID material properties, regardless of the altitude. However, for the TD_3 properties, this holds true only for altitudes exceeding 2500 m, where $M_{cr} > 3$. For $a/h = 125$, the critical Mach numbers are lower than for $a/h = 100$, as expected due to the reduction of the total thickness. Moreover, flutter in the supersonic regime is verified for lower temperature rises, e.g. $\Delta\mathcal{T} = 25$ K. In the case of $\Delta\mathcal{T} = 40$ K and TD_3 material properties, supersonic panel flutter is avoided for $H > 7000$ m, where $M_{cr} > 5$.

It is worth mentioning that since the aerodynamic damping is neglected, the critical Mach numbers are slightly underestimated. Nonetheless, this assumption allows for a more conservative preliminary analysis. Moreover, the boundary layer effects and shock wave interactions are also neglected in the aerodynamic formulation of the quasi-steady First-order Piston Theory [45,47].

4.3. Soft core sandwich panels

The following numerical applications are focused on symmetric sandwich panels composed by a soft core (PVC foam) along with skins made of composite, using unidirectional and curvilinear fibres. Since ESL descriptions provide rather deficient estimations when dealing with soft core sandwich panels [36], only LW models are considered in this subsection.

Regarding the geometric properties, it is considered square panels with in-plane dimensions $a = b = 1$ m, side-to-thickness ratio $a/h = 100$ and core thickness ratio $h_c/h = 0.6$ (each skin made of a single composite layer with $0.2h$ of thickness). The properties of the composite material are the same as in the previous subsection, including the TID, TD_1 and TD_3 material properties, which are also extended for the behaviour of the core material. The TID material properties of the PVC foam, as an isotropic material, are the following [16]: $E = 0.28$ GPa, $\nu = 0.4$, $\alpha = 40\times10^{-6}$ /K, $\rho = 250$ kg/m^3. To include the temperature dependency of the soft core in the TD_1 and TD_3 material properties, the Young modulus is approximated according to the experimental trend provided by Mohammadimehr and Shahedi [13]:

$$E/E_0 = 1.36 - 2.27\times10^{-2}\bar{\mathcal{T}} + 4.24\times10^{-4}\bar{\mathcal{T}}^2 - 3.16\times10^{-6}\bar{\mathcal{T}}^3 \tag{26}$$

where $\bar{\mathcal{T}}$ is the temperature in degree Celsius (°C) and E_0 is the reference Young modulus at the initial reference temperature, which is taken as $E_0 = 0.28$ GPa. In addition, the Poisson coefficient is assumed temperature-independent. The evolution of the Young modulus E and shear modulus $G = E/(2(1+\nu))$ with the temperature is shown in Fig. 4. In the TD_1 material properties, the thermal expansion coefficient of the PVC foam is assumed temperature-independent, whereas in the TD_3 material properties, it is assumed a linear variation with temperature: $\alpha = 40\times10^{-6}(1+\tilde{\alpha}\Delta\mathcal{T})$, where $\tilde{\alpha} = 0.5\times10^{-2}$ /K^2, i.e. in a similar fashion to the TD_3 material properties of the composite material.

Concerning linearized thermal buckling analysis, Fig. 9 presents the critical temperature differences of simply supported sandwich panels with unidirectional fibre composite skins (θ/core/θ) and curvilinear fibre composite skins ($\langle0,\theta_1\rangle$/core/$\langle0,\theta_1\rangle$). More precisely, Fig. 9 parametrically explores the influence of fibre control angles on the thermal buckling stability, with the case of curvilinear fibre composite skins aligning the fibre orientation at the panel centre with the airflow direction (0°) to improve flutter resistance. As previously discussed in the analysis of laminated composite panels, the critical buckling temperatures are overestimated when making use of the TD_1 material properties due to the assumption of temperature-independent thermal expansion coefficients. Conversely, the critical temperatures estimated

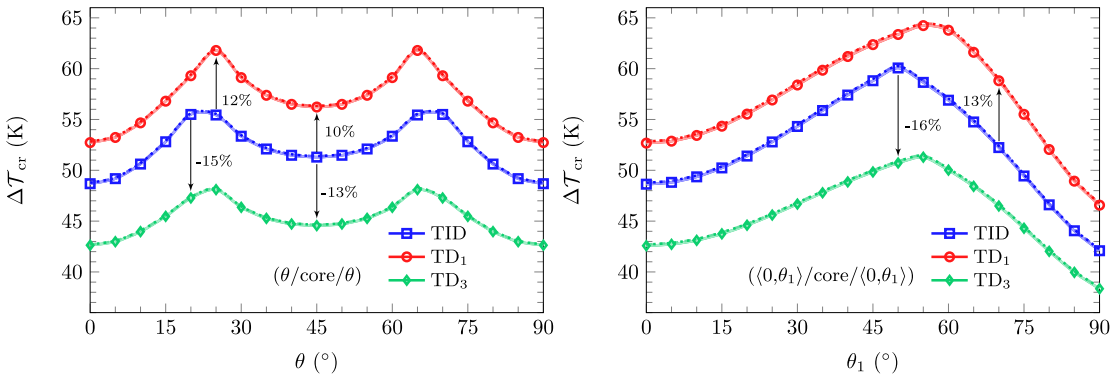

Fig. 9. Critical temperature differences $\Delta\mathcal{T}_{cr}$ of simply supported sandwich panels with unidirectional and curvilinear fibre composite skins: LW FSDT (dotted lines), LW TSDT (dashed lines) and LW Lag3 model (solid lines).

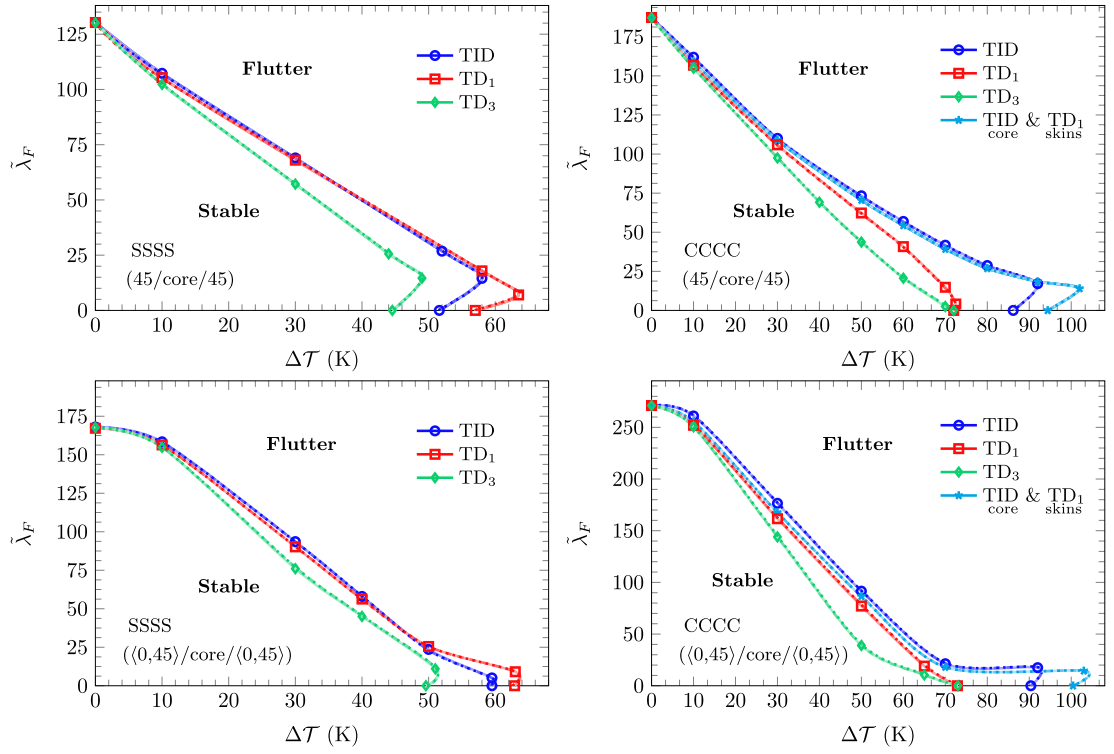

Fig. 10. Evolution of the nondimensionalized flutter pressure parameter $\tilde{\lambda}_F$ with the applied temperature difference $\Delta\mathcal{T}$ of sandwich panels with 45° and $\langle 0, 45\rangle$ composite skins, considering simply supported and clamped boundary conditions: LW FSDT (dotted lines), LW TSDT (dashed lines) and LW Lag3 (solid lines) models.

using the TD$_3$ material properties are lower than those obtained by assuming TID properties, with a maximum discrepancy of −16%.

To enable a meaningful comparison of the aero-thermo-elastic behaviour between conventional and variable stiffness designs, the sandwich panels with unidirectional fibre skins at 45° and curvilinear fibre skins $\langle 0, 45\rangle$ are examined in detail. These configurations provide comparable baseline performance, with standard reference orientations that allow a clear illustration of the benefits offered by fibre steering. Accordingly, considering the (45/core/45) and (⟨0, 45⟩/core/⟨0, 45⟩) sandwich panels, Fig. 10 presents the evolution of the nondimensionalized flutter pressure parameter with the applied temperature difference for both simply supported (SSSS) and clamped (CCCC) boundary conditions. Flutter occurs prevalently due to the coalescence of the first two modes, noting that only the simply supported sandwich panel with $\langle 0, 45\rangle$ composite skins and zero thermal loads experiences flutter due to the third and fourth modes.

In the case of simply supported boundary conditions, Fig. 10 shows that the flutter pressure parameters obtained using the TD$_1$ material properties are close to those derived assuming TID properties, but the panels can endure higher temperature differences without experiencing neither flutter nor buckling, which is explained by the simplified assumption of constant thermal expansion coefficients in the TD$_1$ material properties. Conversely, the inclusion of temperature-dependent thermal expansion coefficients, as in the TD$_3$ material properties, leads to significantly lower flutter and buckling bounds, thus shortening the aero-thermo-elastic stable region.

Up to this point, the temperature rises discussed in the present work are within the temperature ranges involved in the data of the material properties shown in Fig. 4. However, for the clamped sandwich panels explored in Fig. 10, the temperature-dependent behaviour of the core material and the range of temperatures that it can withstand before collapsing play a major role on the aero-thermo-elastic flutter and buckling response. In fact, a comparison of the results derived from the

TID material properties reveals that the critical temperature differences for clamped boundary conditions are greater than for simply supported boundary conditions, as also shown in Table 3 when dealing with the $(\pm\langle 0,45\rangle)_s$ composite panel. To be precise, the critical temperature differences estimated using the TID material properties and clamped boundary conditions are around 90 K, which means that the actual critical temperature is $\mathcal{T}_{cr} = 390$ K, noting that even higher critical temperatures are projected when assuming TID material properties for the core alone and TD_1 material properties for the composite skins. By incorporating the temperature-dependent behaviour of the core, as stated in Eq. (26), the corresponding Young and shear modulus exhibit negative values for temperatures exceeding $\mathcal{T}_{lim} \approx 378$ K and, therefore, the previous thermal buckling predictions with TID material properties are physically inconsistent. Actually, Fig. 4 shows that the Young and shear modulus of the core material decrease significantly for temperatures above 370 K. Hence, unstable vibrations modes arise shortly after $\Delta\mathcal{T} = 70$ K, which limit the curves associated to the TD_1 and TD_3 material properties in the case of clamped boundary conditions.

All in all, the temperature-dependency of the core material critically influences the flutter and buckling behaviour of sandwich panels. Specifically, the PVC foam core exhibits pronounced softening as temperature increases, resulting in sharp reductions in shear modulus above 360–370 K. Therefore, at elevated temperatures, the reduction in both bending and shear stiffness affects the ability of the core to rigidly connect the composite skins and support shear loads, resulting in a significant loss of stiffness and stability as compared to purely composite laminates.

From the structural modelling point of view, the flutter and buckling solutions derived using the LW shear deformation models devoid of thickness stretching align fairly with those obtained resorting to the LW Lag3 model, which includes both high-order transverse normal strains and high-order transverse shear strains. As a result, it is emphasized that the LW FSDT model provides a satisfactory balance between numerical accuracy and computationally efficient for preliminary aero-thermo-elastic stability analysis of sandwich panels experiencing flutter due to the first two modes. Note that the LW FSDT model allows for a reduction of 57% and 70% in the number of DOF as compared to the LW TSDT and LW Lag3 models, respectively, while maintaining a maximum discrepancy around 1%.

For simply supported boundary conditions, Fig. 11 presents the evolution of the critical flutter Mach number with the flight altitude as the applied temperature increases. The results are obtained using the LW Lag3 model, taking into account the TID and TD_3 material properties. Due to the local alignment of the fibres at the centre of the panel with the airflow direction, the sandwich panel with $\langle 0,45\rangle$ composite skins shows higher critical Mach numbers than the sandwich panel with unidirectional fibres at 45°. For example, when considering $\Delta\mathcal{T} = 30$ K and TID material properties, the critical Mach number at sea level, i.e. $H = 0$ m, is $M_{cr} = 2.5$ and 4.0 for the 45° and $\langle 0,45\rangle$ composite skins, respectively. For the TD_3 material properties, the corresponding results are $M_{cr} = 1.8$ and 3.1, which means an average reduction of 25% as compared to the TID material properties. Hence, the variable stiffness sandwich panel under $\Delta\mathcal{T} = 30$ K is capable of flying at, for example, $M_\infty = 3$, without experiencing flutter regardless of the altitude. However, the conventional sandwich panel with unidirectional fibres and TD_3 material properties can only avoid flutter at $M_\infty = 3$ for altitudes above 3000 m, where $M_{cr} > 3$.

The superior aero-thermo-elastic stability of the sandwich panel with $\langle 0,45\rangle$ composite skins over the sandwich panel with composite skins at 45° is justified by the tailored fibre orientations in the variable stiffness configuration. In agreement with available literature on supersonic flutter stability of VSC panels [29,31,42], aligning the fibres with the airflow direction (0° in the present case) improves both axial and bending stiffness parallel to the supersonic airflow direction, delaying mode coalescence and raising the critical flutter pressure parameter. Simultaneously, steering toward 45° at the leading and trailing edges enhances biaxial resistance near the supports, redistributing in-plane stresses more effectively and increasing the critical buckling temperature compared to the uniform 45° orientation. This tailored load redistribution underscores the advantages of variable stiffness designs in sandwich panels under combined thermo-aerodynamic environments.

The flutter mode shapes of the simply supported sandwich panel with $\langle 0,45\rangle$ composite skins are illustrated in Fig. 12, considering $\Delta\mathcal{T} = 0$ K and 30 K. The critical Mach numbers at sea level and corresponding flutter frequencies are also included. For $\Delta\mathcal{T} = 0$ K, flutter occurs due to the coalescence of the third and fourth modes, whereas for $\Delta\mathcal{T} = 30$ K, flutter arises in the first two modes, thus justifying the differences between mode shapes. It is important to note that in the case of $\Delta\mathcal{T} = 30$ K, the in-plane distributions of the flutter mode shapes are very similar for both TID and TD_3 material properties. Even though not shown, the through-thickness distribution of the transverse displacement is approximately constant, even when considering high-order plate theories with thickness stretching, mostly because it is considered a thin sandwich panel with symmetric stacking sequence. In more detail, the flutter mode shapes represented in Fig. 12 are purposefully normalized to exhibit a nondimensionalized maximum transverse displacement of $w_{max}/h = 1$, where h is the total thickness of the panel.

Considering the flutter mode shapes at $\Delta\mathcal{T} = 30$ K, Fig. 13 presents the through-thickness distributions of elastic and thermal (modal) stresses predicted by the various LW models explored in the present work. The elastic and thermal stresses are derived resorting to the stress–strain and stress-temperature constitutive equations, respectively, including the case of TID and TD_3 material properties. Hence, the applied thermal stresses consist of in-plane stresses with constant through-thickness distributions, in agreement with the uniform temperature variation, which are independent of the structural model. The stresses are provided in the following nondimensionalized form:

$$[\tilde{\sigma}_{xx}, \tilde{\sigma}_{yy}] = \frac{h^2}{\bar{\sigma}_0 a^2}[\sigma_{xx}, \sigma_{yy}]$$
$$[\tilde{\sigma}_{xz}, \tilde{\sigma}_{yz}] = \frac{h}{\bar{\sigma}_0 a}[\sigma_{xz}, \sigma_{yz}] \tag{27}$$

where $\bar{\sigma}_0 = 1$ kPa is the reference stress value. The nondimensionalized in-plane normal stresses are provided at the point of maximum transverse displacement, i.e. $\tilde{\sigma}_{xx}, \tilde{\sigma}_{yy}(0.61a, 0.29b)$, whereas the nondimensionalized transverse shear stresses are obtained at the edges, namely $\tilde{\sigma}_{xz}(0, 0.29b)$ and $\tilde{\sigma}_{yz}(0.61a, 0)$.

The main discrepancies among the proposed LW models arise in the evaluation of transverse shear stresses, where high-order effects play a fundamental role, contrasting with the quasi-linear through-thickness distributions of in-plane normal stresses. According to the LW TSDT and LW Lag3 models, the transverse shear stresses can exhibit non-linear through-thickness distributions, as revealed in the case of transverse shear stresses $\tilde{\sigma}_{xz}$. Additionally, these LW models involving cubic z-expansions of displacements are capable of fulfilling approximately the through-thickness continuity of transverse shear stresses demonstrated by the 3D exact elasticity solutions of multilayered panels [16], while predicting almost null transverse shear stresses on the upper and lower surfaces. However, the LW FSDT and LW Lag2 models predict discontinuous through-thickness distributions of transverse shear stresses, which do not satisfy the stress-free conditions on the upper and lower surfaces of the sandwich panel.

Even though the LW FSDT model allows for computationally efficient and numerically accurate flutter solutions in terms of flutter boundaries, high-order LW models with at least cubic z-expansions of in-plane displacements end up necessary for the local analysis of transverse shear stresses in supersonic sandwich panels under flutter conditions. This consideration is highly pertinent to consider in ensuing research regarding the non-linear post-flutter behaviour and failure

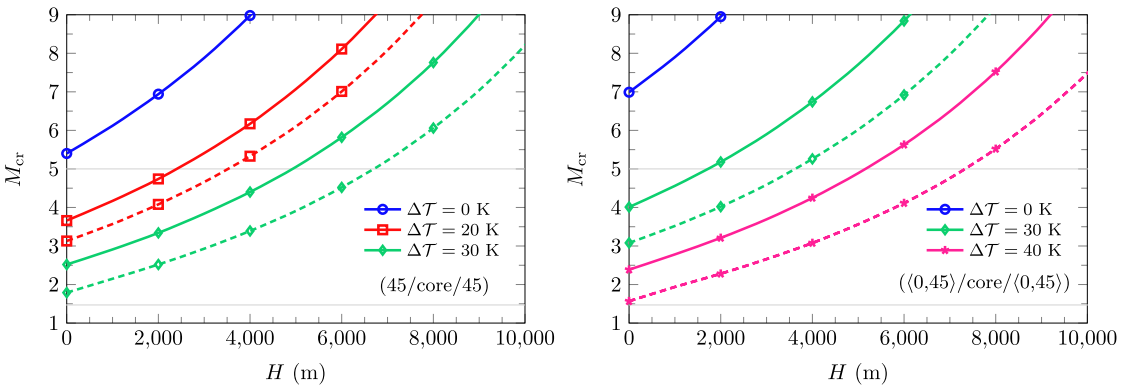

Fig. 11. Evolution of the critical flutter Mach number M_{cr} with the altitude H of simply supported sandwich panels, under increasing temperature differences $\Delta\mathcal{T}$: TID (solid lines) and TD_3 (dashed lines) material properties.

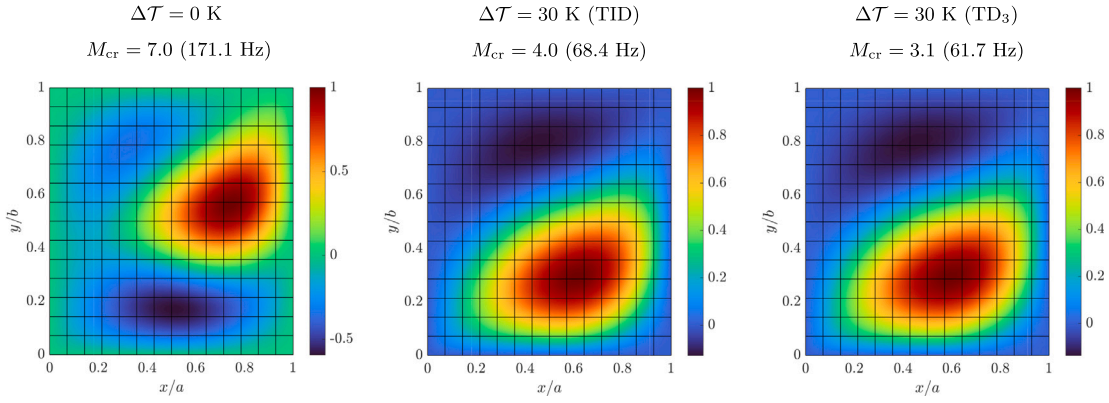

Fig. 12. Flutter mode shapes $w(x, y, 0)/h$ of the simply supported sandwich panel with $\langle 0, 45\rangle$ composite skins, under $\Delta\mathcal{T} = 0$ K and 30 K, considering TID and TD_3 material properties (results obtained at sea level, using the LW Lag3 model).

analysis. Although this study employs the simplified assumption of uniform temperature distributions, more accurate temperature distributions should also be included in future investigations to further assess the impact of temperature-dependent material properties and non-uniform temperature distributions.

Ultimately, it is pointed out that the inclusion of the temperature-dependent material properties associated to the soft core and composite skins is crucial to obtain reliable design optimization studies of sandwich panels for aero-thermo-elastic applications, impacting flutter boundaries and through-thickness distributions of stresses. In addition, the tailoring of curvilinear fibres can be explored in composite laminates and sandwich panels to ensure a good compromise between supersonic flutter resistance and low sensibility to thermal environments.

5. Conclusions

The influence of temperature-dependent material properties on the aero-thermo-elastic stability of multilayered composite panels under supersonic airflow is investigated in this work, considering both variable stiffness laminated composite panels with curvilinear fibres as well as soft core sandwich panels with curvilinear fibre composite skins. Additionally, the numerical accuracy of the linearized thermal buckling and aero-thermo-elastic flutter solutions is assessed by comparing various ESL and LW descriptions, involving either shear deformation plate theories without thickness stretching or further refined theories based on Lagrange z-expansions with thickness stretching, thus making progress on the proper structural modelling and characterization of advanced composite structures for aero-thermo-elastic applications.

As compared to temperature-independent material properties, the assumption of temperature-dependent material properties has a pronounced impact on the aero-thermo-elastic flutter and buckling characteristics of both composite laminates and sandwich panels, which is manifested by lower critical buckling temperatures and lower flutter boundaries. The detrimental impact of the temperature-dependent material properties is not only contingent upon the changes in Young and shear moduli, but also on the variations of the thermal expansion coefficients with the temperature. Moreover, the temperature-dependency of the core material plays a major role on the aero-thermo-elastic response behaviour of sandwich panels, which emphasizes the need for an efficient thermal shielding of critical layers made of highly temperature-sensitive materials. Along with that, composite laminates and sandwich panels with curvilinear fibres can outperform conventional configurations with unidirectional fibres in terms of both thermal buckling resistance and aero-thermo-elastic flutter stability, making them particularly advantageous for high-temperature applications.

Regarding the comparison of the structural models, the application of high-order theories is crucial to ensure highly accurate flutter estimations in composite laminates exposed to temperatures above the critical buckling temperature, especially when dealing with curvilinear fibres and temperature-dependent material properties. In addition, high-order LW models are necessary to accurately capture the through-thickness distributions of transverse shear stresses in soft core sandwich planes under flutter conditions.

In summary, the present study offers new and comprehensive insights into the linear aero-thermo-elastic behaviour and appropriate structural modelling of variable stiffness composite laminates and sandwich panels with temperature-dependent material properties. These

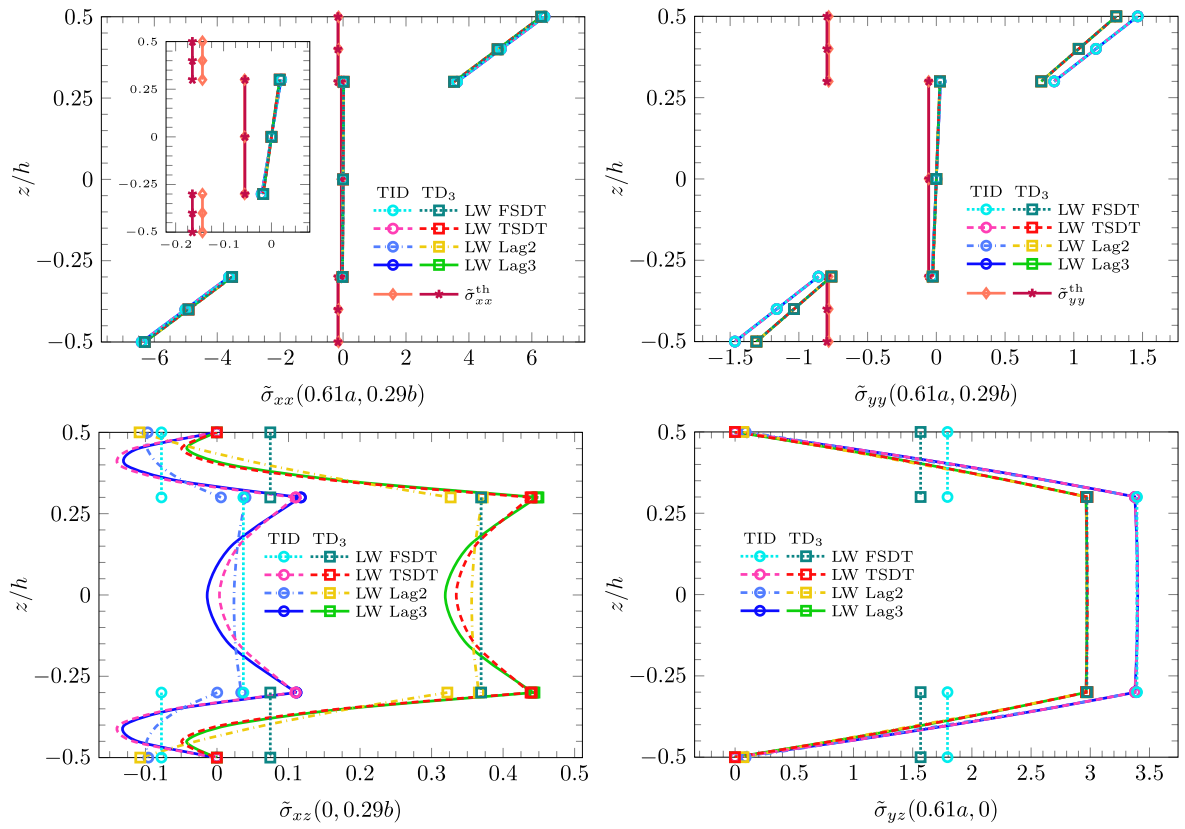

Fig. 13. Through-thickness distributions of nondimensionalized modal stresses in the flutter mode of the simply supported sandwich panel with $\langle 0, 45 \rangle$ composite skin, under $\Delta\mathcal{T} = 30$ K and $M_\infty = M_{\text{cr}}$, considering TID and TD_3 material properties.

findings establish a robust foundation which may be useful for ensuing investigations, particularly extensions to non-linear flutter responses, such as post-flutter limit-cycle oscillations and chaotic behaviours, adapting the temperature-dependent property updates within non-linear solvers. Additionally, the integration of fully coupled aerothermo-elastic formulations with advanced aerodynamic models, including computational fluid dynamics (CFD) methods, represents a promising direction to further enhance predictive accuracy for innovative aerospace structures.

CRediT authorship contribution statement

J.A. Moreira: Writing – review & editing, Writing – original draft, Visualization, Validation, Software, Methodology, Investigation, Funding acquisition, Formal analysis, Data curation, Conceptualization. **F. Moleiro:** Writing – review & editing, Supervision, Methodology, Funding acquisition, Conceptualization. **A.L. Araújo:** Writing – review & editing, Supervision, Methodology, Funding acquisition, Conceptualization. **A. Pagani:** Writing – review & editing, Supervision, Funding acquisition, Conceptualization.

Declaration of competing interest

The authors declare that they have no known competing financial interests or personal relationships that could have appeared to influence the work reported in this paper.

Acknowledgements

The authors acknowledge Fundação para a Ciência e a Tecnologia (FCT) for its financial support via LAETA (project https://doi.org/10.54499/UID/50022/2025). In addition, J.A. Moreira appreciates the financial support of FCT through the PhD Grant 2021.06113.BD (DOI: 10.54499/2021.06113.BD). A. Pagani acknowledges funding from the European Research Council (ERC) under the European Union's Horizon 2020 research and innovation programme (Grant agreement No. 850437).

Data availability

Data will be made available on request.

References

[1] Y. Chai, W. Gao, B. Ankay, F.M. Li, C. Zhang, Aeroelastic analysis and flutter control of wings and panels: A review, Int. J. Mech. Syst. Dyn. 1 (1) (2021) 5–34, http://dx.doi.org/10.1002/msd2.12015.

[2] G.Y. Baghdasaryan, M.A. Mikilyan, L.K. Abbas, P. Marzocca, About the aerothermoelastic stability of panels in supersonic flows, J. Therm. Stresses 36 (9) (2013) 915–946, http://dx.doi.org/10.1080/01495739.2013.788894.

[3] E. Carrera, E. Zappino, K. Patocka, M. Komarek, A. Ferrarese, M. Montabone, B. Kotzias, B. Huermann, R. Schwane, Aeroelastic analysis of versatile thermal insulation (VTI) panels with pinched boundary conditions, CEAS Space J. 6 (1) (2014) 23–35, http://dx.doi.org/10.1007/s12567-013-0054-5.

[4] Z. Chen, Z. Yang, Y. Gu, X. Wang, High-frequency vibration analysis of panels under aerothermoelastic effects in supersonic airflow by an energy finite element method, Thin-Walled Struct. 200 (2024) 111885, http://dx.doi.org/10.1016/j.tws.2024.111885.

[5] L. Librescu, P. Marzocca, W.A. Silva, Linear/nonlinear supersonic panel flutter in a high-temperature field, J. Aircr. 41 (4) (2004) 918–924, http://dx.doi.org/10.2514/1.679.

[6] L. Ye, Z. Ye, Aeroelastic stability and nonlinear flutter analysis of heated panel with temperature-dependent material properties, J. Aerosp. Eng. 33 (6) (2020) http://dx.doi.org/10.1061/(asce)as.1943-5525.0001173.

[7] U. Olsson, Supersonic flutter of heated circular cylindrical shells with temperature-dependent material properties, AIAA J. 16 (4) (1978) 360–362, http://dx.doi.org/10.2514/3.7530.

[8] A. Racionero Sánchez-Majano, A. Pagani, Buckling and fundamental frequency optimization of tow-steered composites using layerwise structural models, AIAA J. 61 (9) (2023) 4149–4163, http://dx.doi.org/10.2514/1.J062976.
[9] A. Pagani, A. Racionero Sánchez-Majano, D. Zamani, M. Petrolo, E. Carrera, Fundamental frequency layer-wise optimization of tow-steered composites considering gaps and overlaps, Aerotec. Missili Spaz. (2024) http://dx.doi.org/10.1007/s42496-024-00212-w.
[10] F. Li, G.J. Nie, Thermo-mechanical buckling analysis of symmetric VAT composite laminates with temperature-dependent material properties, Thin-Walled Struct. 140 (2019) 263–271, http://dx.doi.org/10.1016/j.tws.2019.03.040.
[11] T.A. Guimarães, S.G. Castro, C.E. Cesnik, D.A. Rade, Supersonic flutter and buckling optimization of tow-steered composite plates, AIAA J. 57 (1) (2019) 397–407, http://dx.doi.org/10.2514/1.J057282.
[12] S. Zhang, J.M. Dulieu-Barton, R.K. Fruehmann, O.T. Thomsen, Methodology for obtaining material properties of polymeric foam at elevated temperatures, Exp. Mech. 52 (1) (2012) 3–15, http://dx.doi.org/10.1007/s11340-011-9519-7.
[13] M. Mohammadimehr, S. Shahedi, High-order buckling and free vibration analysis of two types sandwich beam including AL or PVC-foam flexible core and CNTs reinforced nanocomposite face sheets using GDQM, Compos. Part B: Eng. 108 (2017) 91–107, http://dx.doi.org/10.1016/j.compositesb.2016.09.040.
[14] M. Petrolo, E. Carrera, M. Cinefra, E. Zappino, Finite Element Analysis of Structures Through Unified Formulation, John Wiley & Sons, 2014, http://dx.doi.org/10.1002/9781118536643.
[15] F. Moleiro, E. Carrera, G. Li, M. Cinefra, J.N. Reddy, Hygro-thermo-mechanical modelling of multilayered plates: Hybrid composite laminates, fibre metal laminates and sandwich plates, Compos. Part B: Eng. 177 (2019) 107388, http://dx.doi.org/10.1016/j.compositesb.2019.107388.
[16] F. Moleiro, C.M. Mota Soares, E. Carrera, Three-dimensional exact hygro-thermo-elastic solutions for multilayered plates: Composite laminates, fibre metal laminates and sandwich plates, Compos. Struct. 216 (2019) 260–278, http://dx.doi.org/10.1016/j.compstruct.2019.02.071.
[17] R. Vescovini, L. Dozio, Thermal buckling behaviour of thin and thick variable-stiffness panels, J. Compos. Sci. 2 (4) (2018) http://dx.doi.org/10.3390/jcs2040058.
[18] F. Bracaglia, R. Masia, A. Pagani, E. Zappino, E. Carrera, Thermal buckling of variable stiffness composite laminates using high order plate finite elements, Compos. Struct. 345 (2024) 118393, http://dx.doi.org/10.1016/j.compstruct.2024.118393.
[19] F.A. Fazzolari, E. Carrera, Thermo-mechanical buckling analysis of anisotropic multilayered composite and sandwich plates by using refined variable-kinematics theories, J. Therm. Stresses 36 (4) (2013) 321–350, http://dx.doi.org/10.1080/01495739.2013.770642.
[20] P. Nali, E. Carrera, Accurate buckling analysis of composite layered plates with combined thermal and mechanical loadings, J. Therm. Stresses 36 (1) (2013) 1–18, http://dx.doi.org/10.1080/01495739.2012.663679.
[21] H.-S. Shen, Thermal postbuckling behavior of imperfect shear deformable laminated plates with temperature-dependent properties, Comput. Methods Appl. Mech. Engrg. 190 (40) (2001) 5377–5390, http://dx.doi.org/10.1016/S0045-7825(01)00172-4.
[22] M. Shariyat, Thermal buckling analysis of rectangular composite plates with temperature-dependent properties based on a layerwise theory, Thin-Walled Struct. 45 (4) (2007) 439–452, http://dx.doi.org/10.1016/j.tws.2007.03.004.
[23] M.K. Singha, L.S. Ramachandra, J.N. Bandyopadhyay, Thermal postbuckling analysis of laminated composite plates, Compos. Struct. 54 (4) (2001) 453–458, http://dx.doi.org/10.1016/S0263-8223(01)00117-9.
[24] W. Zhao, K. Singh, R.K. Kapania, Thermal buckling analysis and optimization of curvilinearly stiffened plates with variable angle tow laminates, J. Spacecr. Rockets 56 (4) (2019) 1189–1204, http://dx.doi.org/10.2514/1.A34378.
[25] G. Jiang, F. Li, Aerothermoelastic analysis of composite laminated trapezoidal panels in supersonic airflow, Compos. Struct. 200 (2018) 313–327, http://dx.doi.org/10.1016/j.compstruct.2018.05.138.
[26] F.-M. Li, Z.-G. Song, Aerothermoelastic analysis of lattice sandwich composite panels in supersonic airflow, Meccanica 51 (2013) 887–891, http://dx.doi.org/10.1007/s11012-015-0240-y.
[27] W. Yu, R. Guo, Y. Zhao, M. Chen, Isogeometric flutter analysis of a heated laminated plate with and without cutout, Thin-Walled Struct. 206 (2025) 112652, http://dx.doi.org/10.1016/j.tws.2024.112652.
[28] J. Zhang, Y. Qu, F. Xie, Z. Peng, W. Zhang, G. Meng, Investigations on nonlinear aerothermoelastic behaviors of multilayered composite panels subject to frictional boundaries and random acoustic loads in supersonic flow, Thin-Walled Struct. 158 (2021) 107180, http://dx.doi.org/10.1016/j.tws.2020.107180.
[29] X. Ouyang, Y. Liu, Flutter of variable stiffness composite laminates in supersonic flow with temperature effects, J. Compos. Mater. 55 (23) (2021) 3253–3266, http://dx.doi.org/10.1177/00219983211007542.
[30] Y. Gao, J. Duan, Y. Lei, B. Xu, Aerothermoelastic analysis of curvilinear fiber variable stiffness laminated panels in supersonic flow, Acta Mech. 233 (2022) 4327–4345, http://dx.doi.org/10.1007/s00707-022-03331-2.
[31] J. Gong, C. Zhang, F. Xin, Aerothermoelastic flutter analysis of variable angle tow composite laminated plates in supersonic flow, Appl. Math. Model. 130 (2024) 119–139, http://dx.doi.org/10.1016/j.apm.2024.02.024.
[32] X. Chen, G. Nie, Nonlinear thermal flutter analysis of variable angle tow composite curved panels in supersonic airflow, Compos. Struct. 277 (2021) 114610, http://dx.doi.org/10.1016/j.compstruct.2021.114610.
[33] G. Nie, H. Li, X. Chen, Nonlinear thermal flutter of variable angle tow curved panels with elastically restrained edges in supersonic airflow by generalized Galerkin method, J. Compos. Mater. 59 (6) (2025) 835–851, http://dx.doi.org/10.1177/00219983241300147.
[34] Y. Yan, L. Zhang, Variable-kinematic finite elements for the aero-thermo-elastic analysis of variable stiffness composite laminates, Mech. Adv. Mater. Struct. (2022) 1–17, http://dx.doi.org/10.1080/15376494.2022.2119312.
[35] J.A. Moreira, F. Moleiro, A.L. Araújo, A. Pagani, Equivalent single layer and layerwise models for flutter and buckling analysis of supersonic variable stiffness laminated composite plates, Thin-Walled Struct. 191 (2023) 111012, http://dx.doi.org/10.1016/j.tws.2023.111012.
[36] J.A. Moreira, F. Moleiro, A.L. Araújo, A. Pagani, Layerwise models for supersonic flutter analysis of viscoelastic sandwich panels with curvilinear fibre composite skins, J. Sound Vib. 572 (2024) 118182, http://dx.doi.org/10.1016/j.jsv.2023.118182.
[37] J.A. Moreira, F. Moleiro, A.L. Araújo, A. Pagani, Active aeroelastic flutter control of supersonic smart variable stiffness composite panels using layerwise models, Compos. Struct. 343 (2024) 118287, http://dx.doi.org/10.1016/j.compstruct.2024.118287.
[38] J.A. Moreira, F. Moleiro, A.L. Araújo, A. Pagani, Active aero-visco-elastic flutter control and layerwise modelling of supersonic smart sandwich panels with variable stiffness composites, Aerosp. Sci. Technol. 157 (2025) 109847, http://dx.doi.org/10.1016/j.ast.2024.109847.
[39] J.A. Moreira, F. Moleiro, A.L. Araújo, A. Pagani, Aero-thermo-elastic stability analysis of supersonic variable stiffness sandwich panels using refined layerwise models, Compos. Struct. 357 (2025) 118920, http://dx.doi.org/10.1016/j.compstruct.2025.118920.
[40] Y. Chai, F. Li, Z. Song, Nonlinear vibrations, bifurcations and chaos of lattice sandwich composite panels on Winkler–pasternak elastic foundations with thermal effects in supersonic airflow, Meccanica 54 (7) (2019) 919–944, http://dx.doi.org/10.1007/s11012-019-00995-4.
[41] Z. Gürdal, R. Olmedo, In-plane response of laminates with spatially varying fiber orientations - Variable stiffness concept, AIAA J. 31 (4) (1993) 751–758, http://dx.doi.org/10.2514/3.11613.
[42] H. Akhavan, P. Ribeiro, Aeroelasticity of composite plates with curvilinear fibres in supersonic flow, Compos. Struct. 194 (2018) 335–344, http://dx.doi.org/10.1016/j.compstruct.2018.03.101.
[43] J.N. Reddy, Mechanics of Laminated Composite Plates and Shells – Theory and Analysis, second ed., CRC Press, Boca Raton, 2004.
[44] W.T. Koiter, A consistent first approximation in the general theory of thin elastic shells, in: Proceedings of First Symposium on the Theory of Thin Elastic Shells, North-Holland, Amsterdam, 1959, http://resolver.tudelft.nl/uuid:13cb5366-bbdc-4dd1-8514-951302217759.
[45] Y.-Y. Chai, Z.-G. Song, F.-M. Li, Active aerothermoelastic flutter suppression of composite laminated panels with time-dependent boundaries, Compos. Struct. 179 (2017) 61–76, http://dx.doi.org/10.1016/j.compstruct.2017.07.053.
[46] Y. Yan, A. Pagani, E. Carrera, Thermal buckling solutions of generic metallic and laminated structures: Total and updated Lagrangian formulations via refined beam elements, J. Therm. Stresses 45 (8) (2022) 669–694, http://dx.doi.org/10.1080/01495739.2022.2090471.
[47] E.H. Dowell, Panel flutter - a review of the aeroelastic stability of plates and shells, AIAA J. 8 (3) (1970) 385–399, http://dx.doi.org/10.2514/3.5680.